HVDC TRANSMISSION SYSTEM RELIABILITY EVALUATION BASED ON CONDITION-DEPENDENT FAILURE MODELS OF CONVERTERS AND TRANSFORMERS

by

Zibo Wang

A Thesis Submitted in

Partial Fulfillment of the

Requirements for the Degree of

Master of Science

in Engineering

at

The University of Wisconsin-Milwaukee

May 2017

ABSTRACT

HVDC TRANSMISSION SYSTEM RELIABILITY EVALUATION BASED ON CONDITION-DEPENDENT FAILURE MODELS OF CONVERTERS AND TRANSFORMERS

by

Zibo Wang

The University of Wisconsin-Milwaukee, 2017
Under the Supervision of Dr. Lingfeng Wang

Wind energy, especially offshore wind energy, is the focus of policy for countries that want to make significant use of renewable energy. With the development of semiconductor technology, high voltage direct current (HVDC) technology is being widely used for the transmission of wind power from offshore windfarms to onshore power grids. The application of HVDC technology can benefit the power system in many ways, such as operation security, reliability performance and economy. With the increasing number of applications of HVDC, the reliability performance of HVDC plays an important role in the overall power system reliability. Although the reliability of HVDC transmission system has been studied for some time, most of the research is only for the reliability evaluation of the planning stage, but the evaluation of operational reliability is rarely mentioned.

Converters and transformers are major components in VSC-HVDC transmission systems. Constant failure rate for components (transformers and converters) has been proven to be feasible and it is widely used in power system to calculate medium or long term average reliability indices [23]. Constant failure rate is an average value for long-time. However, the average failure rates cannot

represent the components' failure probability under different operating conditions and operating environment.

In this thesis, a converter real-time failure model and a transformer real-time failure model were built and tested. These two models were applied to two VSC-HVDC transmission systems (radial, regional) to calculate the operating reliability indices. And a set of sensitivity analyses was conducted to evaluate the influence of various factors.

The converter real-time failure model is based on the power loss of power electronics which is caused by the wind speed and its variation, and the influence of ambient temperature was considered. For the transformer real-time failure model, the aging failure caused by the mechanical strength loss, the random failure based on weather condition and the failure caused by overload protection was considered. To calculate the operating reliability for two systems, systems were simplified by using the minimum cut set method. Combined with the real-time availability of the transformer and the converter, and other components, the system hourly reliability was calculated. In the calculation, the difference between offshore and onshore was considered. The sensitivity analyses demonstrated the influence of season, DC cable capacity, and wind turbine parameters.

According to the calculation results, the reliability of the major components can be more accurately reflected by these condition-dependent models. The availability for the system varies evidently with different operating and environment conditions. The ambient temperature and the wind speed are the main affecting factors. The one-year simulation results demonstrate that the system reliability exhibits some degree of seasonal nature. Also, it was shown that the system topology, DC cable capacity, and wind turbine parameters could affect the system reliability.

TABLE OF CONTENTS

LIST OF FIGURES

LIST OF TABLES

ACKNOWLEDGEMENTS

First of all, I would like to thank my thesis advisor Dr. Lingfeng Wang for his patience and generous support. Without his continuous guidance on my research, this thesis would not have been possible. Dr. Wang has deeply touched me with his rigorous attitude toward research and his unwavering commitment to performing high-level research. His professional mentorship throughout my study here will have a profound impact on my future profession.

I would also like to thank my thesis committee: Drs. Chiu Tai Law and Dr. Wei Wei for their guidance and comments. Also I thank them for their time from their busy schedule. They are my role models in my future study.

Additionally, I want to express my sincere gratitude to my labmates, Yingmeng Xaing, Jun Tan, for their advice in my research and other friends for their company and support.

Last but not least, I want to thank my parents for their support and love.

.

Chapter 1 Introduction

1.1 Research Background

Fossil energy has long supported the development and progress of human society. The International Energy Agency (IEA) survey in 2014 showed that 2013 fossil energy subsidies totaled US$550 billion. It was four times that of renewable energy [1]. Compared with fossil fuels, renewable energy resources are eco-friendly, low-cost and plentiful. Wind energy, especially offshore wind energy, is the focus of policy for countries that want to make significant use of renewable energy.

The transmission of wind power from offshore windfarms to onshore power grids is through either high voltage alternating current (HVAC) technology or high voltage direct current (HVDC) technology. In reference [2], the economical and reliability analysis between HVDC and HVAC was carried out. The results showed the choice of transmission scheme is largely dependent on the distance from offshore windfarms to onshore. Because the HVDC scheme needs more investment for components, the HVAC scheme needs more investment for cable.

Although HVAC technology is widely used worldwide to be the main scheme for electrical transmission for the past 100 years, it still has its limitations, such as transmission capacity, distance constraints and inability to connect asynchronous grids. With the advent of renewable energy and the need to build more smart grids, HVDC transmission is no longer a supplement to HVAC transmission. HVDC is widely used for subsea electrical transmission, interconnection of asynchronous AC grids, efficient, stable control and transmission capability and also for long-distance bulk power transmission because of its low power loss [3].

1.1.1HVDC transmission system and its main components

High Voltage Alternating Current (HVAC) technology has been the dominant method for power

transmission for a long time. Presently, there are certain areas in which High Voltage Direct Current (HVDC) can be a suitable method for power transmission. HVDC transmission is often used for long-distance, high-capacity transmission and interconnection between regional power grids. It converts the alternating current into direct current through the inverter and then sends it to the receiving terminal through the DC transmission line and becomes alternating current through the inverter, and finally injected into the AC grid. Relative to HVAC transmission, the HVDC transmission has advantages of flexible transmission, small loss, lines saving, rapid control and so on.

The first application of HVDC dates back to the 1950s. Based on the development of converters, there has been three stages for HVDC transmission system. The first stage is widely known by the application of mercury arc valve. Since the 1970s, silicon controlled rectifiers (SCR) take the main market of HVDC converters [4]. In the late 1990s, with the development of semiconductor technology, Voltage Source Converters (VSC) start to emerge in industrial applications[4].

Based on thyristor and transistor technology development, the fully controlled semiconductor devices for high-voltage and high-power are available today (Table 1-1). These devices are widely used for Voltage Source Converters with pulse width modulation (PMW) working at higher frequency [5].

Acronym	Type	Full Name
IGBT	Transistor	Insulate Gate Bipolar Transistor
IEGT	Transistor	Injection Enhanced Gate Transistor
GTO	Thyristor	Gate Turn-off Thyristor
IGCT	Thyristor	Integrated Gate Commutated Thyristor
GCT	Thyristor	Gate Commutated Turn-off Thyristor

Table 1-1Summary of fully controlled high-power semiconductors

Until 2009 about 100 HVDC schemes are operating or planned to be installed worldwide. More than 80 GW of the power is delivered via CSC (Current Source Converter) or VSC (Voltage Source Converters) scheme [5]. Table 1-2 illustrates the differences between CSC and VSC.

Scheme	Semiconductor	Power Level
CSC-HVDC	Thyristors	around 1000 MW
VSC-HVDC	GTO/IGBT	300-400 MW

Table 1-2 Two scheme for HVDC

The basic configuration of these two schemes is shown below, CSC-VHDC technology has been relatively mature, and so far, the technology has been constantly improved. VSC-VHDC has received extensive attention in recent years.

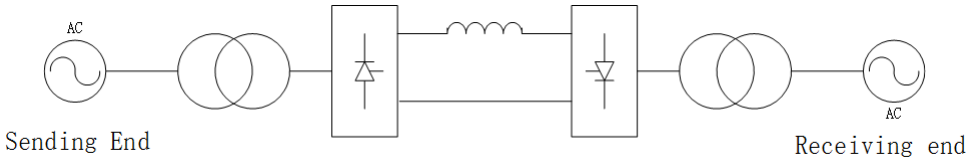

Figure 1-1 CSC-HVDC system based on thyristors

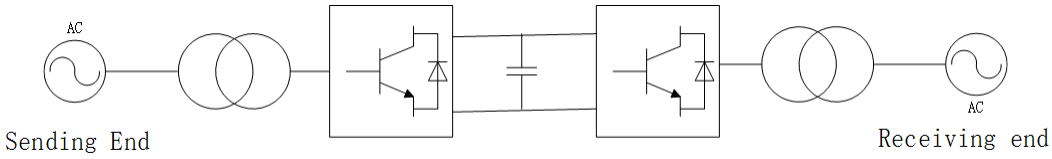

Figure 1-2 VSC-HVDC system based on IGBTs

Compared to Line Commuted Source Converters based on HVDC, VSC-HVDC system is more suitable for specific applications, such as small isolated remote loads, offshore generation and power supply to island [6], [7]. And VSC-HVDC is more suited for offshore generation because it does not need a strong AC system and has a smaller footprint in comparison to CSC-HVDC [8].

Because the DC inductor can help limit the current, the CSC has the ability to resist short circuits under fault conditions. VSC is more likely to be damaged due to line failure, so in the VSC-HVDC application, the choice of cable is more important. With the improvement of the cable production process, VSC-HVDC has received more and more attention [9]. The DC side fault of the VSC-HVDC system can be solved by circuit breakers (CB) [10]. In the case of VSC loss the advanced DC voltage controller can solve the problem of power excess. The advantage of VSC-HVDC is listed below:

1.VSC current can be self-shut off, and VSC can work in the passive inverter mode, with no need for additional commutation voltage, thus overcoming the traditional flaw that HVDC receiver must be fundamental to the active network. The use of HVDC for remote isolation Load transmission is possible.

2. Normal operation VSC can simultaneously and independently control active and reactive power. The control can be more flexible and convenient.

3. VSC not only does not need to provide reactive power on the AC side, but also can play the role of STATCOM, that is, dynamic compensation for the reactive power for AC bus, stable AC bus voltage. This means that the VSC-HVDC system can provide emergency support for active power to the fault area and emergency support of reactive power if the VSC capacity is allowed to be tolerated, thus improving the system's voltage and power angle stability.

4. DC current reverses when the power flow reverses direction, while the DC voltage polarity

remains unchanged, to which the traditional HVDC is exactly the opposite. This feature is conducive to the parallel multi-terminal DC system formation by being both easy to control the trend and having a higher reliability.

5. As the VSC AC side current can be controlled, it will not increase the system short-circuit capacity. This means that after the addition of the new VSC-HVDC line, the protection of the AC system does not need to be changed.

6. VSC usually uses SPWM technology and the switching frequency is relatively high. After low-pass filter can get the required AC voltage, the required capacity of the filter device is also greatly reduced.

An illustration of the two-level converter is shown in Figure 1-3

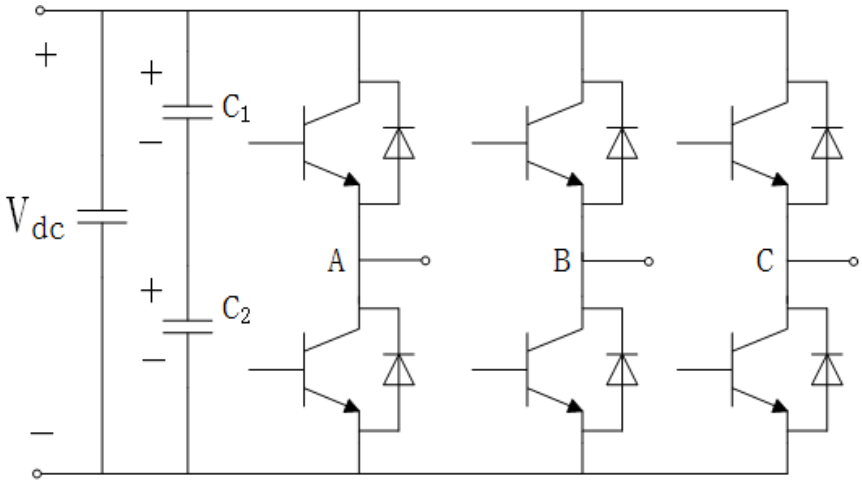

Figure 1-3 Illustration of the two-level converter

As shown above, each VSC consists of 6 diodes and 6 IGBTs, and each phase leg of the converter connects to the AC system through a reactor. Filters on the AC side are used to reduce the harmonic

content flowing to the AC side.

The DolWin beta project [11] commissioned in 2017 in the North Sea of Germany is the world's most powerful offshore converter station to date. Its transmission capacity is 916 megawatts (MW), the voltage level is 320-kilovolt and the transmission distance is 135km (45km submarine cable and 90km underground cable). It is able to transmit the clean energy to around 1,000,000 households.

Electric transformer is important substation equipment in the electrical power system. It is the core component in both HVAC and HVDC transmission systems. Power transformers transform high voltage power to low voltage power, and provides electric service to terminal users in power distribution systems. Nowadays, the majority of servicing transformers are oil-filled transformers, which have complex structure and are vulnerable to bad weather conditions. The reliability of a transformer is of significant importance for industry to improve the level of safe operation and maintenance [12].

Overloading of a power transformer will increase depreciation cost and reduce its physical lifetime because it accelerates a transformer's insulation aging. Moreover, overloading also increases the failure risk of the transformer which may cause cascading outages and frequent interruptions in power systems [13]. References [14], [15], [16] studied the weather-dependent failure rate of weather-exposed components, the real-time load model was built, and transmission and distribution system reliability calculation was also included. In [17], the influence of the hottest temperature (HST) on the insulation life of the transformer was studied. The potential risk of bubble discharge under severe overload conditions was also studied. In [18], the outage risks of transformers

under overloading conditions were studied. The influence of ambient temperature and real-time load for an overloading transformer was studied in reference [19]. Reference [13] proposed a hybrid conditions-dependent outage model (CDOM) for a transformer. The CDOM considers three failure models: the aging failures due to rising HST which will damage the mechanical strength of conductor; the random failures due to weather conditions, which is set as a weather-dominant failure rate model; and the overload protection outage model considering the outages caused by the direct trips of the overload protection. However, when evaluating the system's reliability other components' real-time failure rate is not considered. That paper analyzes the reliability indexes based on the CDOM model for a traditional AC power system, but the application for an HVDC system is not mentioned. For the HVDC system converter's operating condition is even more essential than the transformer. To calculate the HVDC system real-time reliability, a converter's operating reliability model should be built [20], [21].

1.1.2HVDC transmission system reliability

The application of HVDC technology can benefit the power system in many ways, such as operation security, reliability performance and economy [22]. With the increasing number of applications of HVDC, the reliability performance of HVDC plays an important role in power system reliability. The reliability evaluation of HVDC systems first emerged in the 1970s, when mercury arc valves were widely used and also at that time thyristor-based SCRs were starting to become available. Reference [23] is one of the earliest studies in HVDC reliability area, analyzing the reliability and availability of HVDC station with thyristor-based SCRs. Different power components in the HVDC system and their impact on the system reliability was analyzed in reference [24]. After the 2000s, new technology has been available for the HVDC transmission system, such as voltage source converter (VSC), ultra HVDC, and multiterminal HVDC. Reference [25] is the

earliest paper to analyze the reliability of multiterminal HVDC transmission systems. Reference [26] studied the reliability of HVDC systems with different topologies, the results of the study show that HVDC systems are vulnerable to high-impact and low-probability faults. Reference [22] uses a state-enumerated approach to extend the reliability evaluation to ultra HVDC systems, and introduced two new reliability indices for HVDC systems.

Although the reliability of HVDC transmission system has been studied for some time, most of the research is only for the reliability evaluation of the planning stage, but the evaluation of operational reliability is rarely mentioned. Constant failure rate for components (transformers and converters) has been proven to be feasible and it is widely used in power system to calculate medium or long term average reliability indices [23]. Constant failure rate is an average value for long-time. However, the average failure rates cannot represent the components' failure probability under different operating conditions and operating environment.

HVDC transmission system's reliability with a VSC station is studied in [27]; in [28], the reliability of HVDC converter is further studied. Reference [29] evaluates reliability of a small wind turbine power converter system. That paper only considered the relationship between power loss and components' failure rates, but impacts of the system's operating states were missed. The operating states mainly influenced by random variations of wind speed. Reference [30] provides a model of real-time failure rate evaluation for converters in HVDC transmission systems. The result shows that the operational reliability evaluation considering the real-time operational states of the system is especially suitable to evaluate the reliability of a system with factors that affect its reliability on a real-time basis, like the HVDC transmission system that connects a wind farm and the main grid. However, reference [30] only presents the operating reliability for a converter system; it does not

analyze the impact on a specific transmission system based on converter's real-time failure rate. And other important components, such as a transformer's operating reliability are still not taken into consideration.

1.2 Reliability Evaluation Method

The reliability evaluation method for electric power systems can be classified into two categories: simulation method and analytical method [23].

1.2.1 Simulation Method

The simulation method mainly refers to the Monte Carlo (MC) simulation, which estimates the reliability indices by simulating the random process and actual process of the system. MC method can be mainly divided into time sequential MC method and non-sequential MC method. Non-sequential Monte Carlo simulation is often called state sampling method. The sampling of the system is based on a state where the system state is the state of all the originals, and the state of each element can be determined by sampling the probability of occurrence in particular in that state. The sequential Monte Carlo simulation is a simulation of the elements' state in a time span according to the timing. Among them, there are different ways to establish the virtual system state transition cycle. The most commonly used methods include state duration sampling method, system state transition sampling method and so on.

Monte Carlo simulation is a simple and easy way for system reliability evaluation, however, this method costs too much time and resources. And, it cannot evaluate the reliability sensitivity directly. This method is mainly used to calculate mid-size and big systems.

1.2.2Analytical Method

The analytical method focuses on calculating the reliability index using direct numerical method, such as Fault Tree Analysis (FTA) and Frequency and Duration method (FD method). Fault tree method is a method of using graphical deductive logic reasoning, using the diagram to explain the cause of the system failure. FTA combines the system failure with component failure, by finding all the possible failures of the system, that is, all the smallest cut sets of the fault tree. Fault tree is visual technical information; when it is completed, it is an intuitive design and maintenance guide for the operators and designers. As the transmission capacity of HVDC transmission system is large, the original parts are large, the structure is complex and the operation mode is varied. The fault tree modeling workload is huge and the calculation result has some error.

FD method focuses on establishing the state space diagram of the subsystems and obtaining the reliability equivalent model to establish the state space diagram of the whole HVDC system. Because HVDC transmission system is complex, the dimension of states is large, the drawing of state space diagram is cumbersome and error prone. In addition, when the original transfer relationship and the system structure changes, there is the need to re-establish the reliability model.

The basic idea of the serial-parallel network analysis method is to describe the structural characteristics of the DC transmission system. The capacity model can be expressed as a series-parallel combination of the capacity model of each subsystem. Therefore, as long as the capacity model and its serial and parallel combination is known, the DC system capacity model can be built.

In this paper the definition of in series and parallel is based on reliability point of view. Also it can be explained as based on the relationship between system failure (success) and components failure

(success).

For a series system, the system fails if any of the components in the system fail. In other words, all the components must work properly, so the system can work properly. This system is called the series system.

Figure 1-4 Series system of two components

A series system consisting of two independent components is shown in Figure 1-4. In this system, component A and component B must both operate before the system function can be realized. The failure rate for series system consists of n components calculated as follows:

$$\lambda_s = \sum_{i=1}^{n} \lambda_i \tag{1.1}$$

For a parallel system, the system fails if all components of the system fail. In other words, if any one of the components work, the system can work properly. This system is called the parallel system.

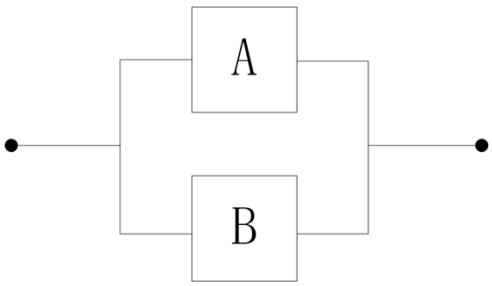

Figure 1-5 Parallel system of two components

A parallel system consisting of two independent components is shown in Figure 1-5. In this system, only if component A and component B fail does the system fail. The repair rate for parallel system consisting of n components is calculated as follows:

$$\mu_s = \sum_{i=1}^{n} \mu_i \tag{1.2}$$

The minimum cut set method is a basic concept of Fault Tree Analysis; by using this method we can simplify a complex system to a simple series and parallel system, and to calculate its reliability. The minimum cut set is actually a set of such components together: when these components are removed from the network, the power supply path of the load point is all cut off, and when any of the components are returned, the load point restores at least one power supply path. It is shown in Figure 1-5, where we can see that the minimum cut set from source 1 to load 4 is (A, D), (B, E), (A, C, E), (B, C, D). By using the concept of fault tree we can simplify the system in Figure 1-5 to Figure 1-6, since only if all the components in a minimum cut set stop working the system fail, they are in parallel connection. And if any cut set happens the system fails, so all the cut set is in series.

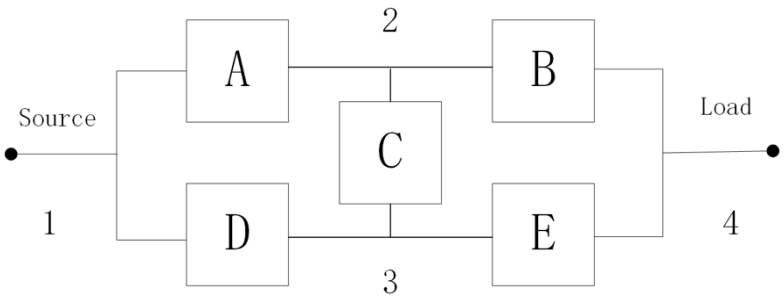

Figure 1-5 Model of meshed network

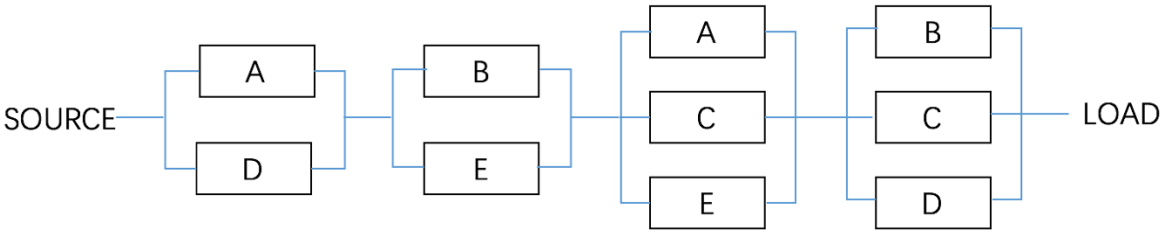

Figure 1-6 network after minimum set simplify

1.3 Research Objective and Thesis Layout

The main goal of this thesis is to evaluative the HVDC system real-time reliability, considering its main components' real-time failure rate. A converter's real-time failure model and a transformer's failure model will be built. For converter real-time failure model, the effect of wind speeds operating condition and ambient temperature is considered. For transformer real-time failure model, aging failure caused by the mechanical strength loss, random failure based on weather condition and failure caused by overload protection is taken into consideration. The models are applied to different HVDC transmission schemes, and the sensitivities analyses are made to compare the real-time indexes to constant indexes, and other influences.

In this thesis, a converter real-time failure rate model considering wind speeds and operating environment is proposed and tested in chapter 2, a transformer conditions-dependent outage model considering aging failure caused by the mechanical strength loss, random failure based on weather condition and failure caused by overload protection is proposed and tested in chapter 3. Further, the real-time reliability of two HVDC transmission schemes based on components' operating reliability model is studied in chapter 4. And the sensitivities analysis is proposed in chapter 5; The conclusions are presented and future work is prospected in chapter 6.

Chapter 2 A Converter Real-time Failure Model

2.1 Introduction

To evaluate the reliability of power electronics, two methods are widely used. One is an empirical reliability model, while another is a physics-based reliability model. The former largely relies on historical operating data, but the current running VSC-HVDC does not have enough data to support reliability analyses. The latter evaluates reliability based on the specific operational states and operating environment.

Reference [30] provides a model of real-time failure rate evaluation for converters in HVDC transmission systems. This paper built on the multi-level failure rate model of wind turbine power converter system (WTPCS) based on the power loss of power electronic devices. However, the literature established by the multistate failure model cannot fully show the component's hourly failure rate. Moreover, the study only takes the converter and its necessary equipment into account and does not analyze at the transmission system level.

In this chapter a converter real-time failure rate model considering the effect of wind speed is built. This model is based on the power loss of power electronics which is caused by the wind speed and its variation. Also the influence of ambient temperature is considered.

The remainder of this chapter is organized in the following way. The real-time converter failure rate model is presented in section 2.2. The parameter setting and model test are presented in section 2.3. The summary of this chapter is given in section 2.4.

2.2 Model Establishment

In this model, the failures caused by thermal over-temperature and failures caused by thermal cycling [31] are considered. Because of the fluctuations of wind speed, wind farm generation varies from time to time. Thus, the power loss of power electronics will cause the temperature rise of the components and cause the components' failure. The logic diagram of this model is shown below.

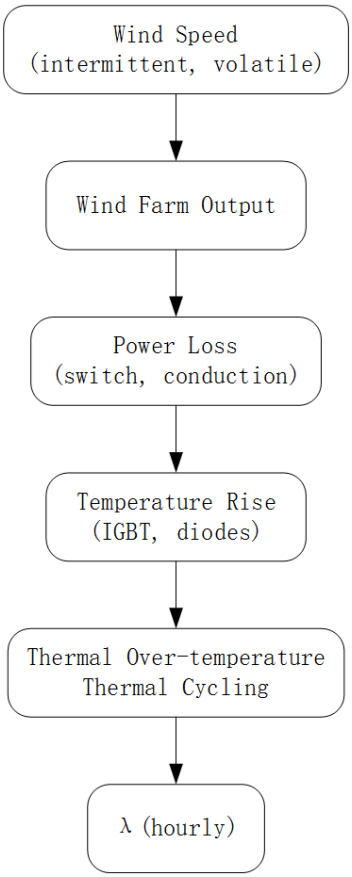

Figure 2-1 Real-time converter outage model

As shown in Figure 2-1, this failure rate model of a VSC is to a great extent influenced by the real-time wind speed. In other words, if we input the hourly wind speed and hourly ambient temperature into this model we can calculate the real-time failure rate.

2.2.1 Calculating Output Power

First the relationship between the wind speed and windfarm output is presented. The output of the wind farm is directly affected by the wind speed [32]. The relationship between them is as follows:

$$P_w = \begin{cases} P_{wr} & v_r \le v < v_{co} \\ P_{wr} \times \frac{v - v_{ci}}{v_r - v_{ci}} & v_{ci} \le v < v_r \\ 0 & others \end{cases} \quad (2.1)$$

As shown above P_w is the power output of the wind turbine, P_{wr} is the wind turbine rated output, v is the wind speed, and v_{ci} and v_{co} are the cut-in and cut-out wind speed. Obviously, when the wind speed exceeds a cut-out speed, the turbine output remains constant. When the wind speed is below cut-in speed, the turbine stops working. It is worth noting that the cut-in speed effects not only the time to put into operation, different cut-in speed settings also affect the wind turbine efficiency during normal operation.

2.2.2 Calculating the Power Loss of Converter

In this paper we considered the traditional two-level three-phrase converter with 6 IGBTs and 6 diodes. According to the operating characteristics of the VSC, the power loss of the VSC is the power loss of each diode or IGBT in the VSC. These losses can be calculated according to the output power, voltage and frequency of the wind turbine [Effect of Wind Speed on Wind Turbine Power Converter Reliability]. The loss on diode and IGBT can be expressed as follows [33], [34]:

$$P = V_{diode} I \left(\frac{1}{2\pi} \mp \frac{M}{8}\cos\theta\right) + R_{diode} I^2 \left(\frac{1}{8} \mp \frac{M}{3\pi}\cos\theta\right) + \frac{f}{\pi} \cdot \frac{V_{DC} I}{V_{ref,diode} I_{ref,diode}} E_{diode} \quad (2.2)$$

$$P = V_{IGBT} I \left(\frac{1}{2\pi} \pm \frac{M}{8}\cos\theta\right) + R_{IGBT} I^2 \left(\frac{1}{8} \pm \frac{M}{3\pi}\cos\theta\right) + \frac{f}{\pi} \cdot \frac{V_{DC} I}{V_{ref,IGBT} I_{ref,IGBT}} E_{on} + E_{off} \quad (2.3)$$

in which V_{diode} and V_{IGBT} are the voltage drops across the diode and IGBT; R_{diode} and R_{IGBT} are the conduction resistance of the diode and IGBT respectively; E_{diode} is the rated switching loss on the diode, E_{on} and E_{off} are the power losses of IGBT during the operation; V_{DC} is DC link voltage; $V_{ref,diode}$ and $V_{ref,IGBT}$ are the reference commutation voltage of diode and IGBT; $I_{ref,diode}$ and $I_{ref,IGBT}$ are the reference commutation current of diode and IGBT; M is the modulation index; and θ is the angle between the current and voltage. In Equation (2.2) and (2.3) I is the peak phase current that can be expressed by[33]:

$$I \approx \frac{\sqrt{2} P_t}{\sqrt{3} U_l} \quad (2.4)$$

Where P_t is the power output from the wind turbine and U_l is the line-to-line voltage on the AC side.

The total power loss of the converter can be calculated by

$$P_{loss} = \sum_{i=1}^{N1} P_{IGBT,i} + \sum_{j=1}^{N2} P_{diode,j} \quad (2.5)$$

in which $N1$ is the number of IGBTs in the converter and $N2$ is the number of diodes in the converter. The temperature rise in the converter can be calculated as below [33]:

$$T_{module} = T_{ambient} + R_{ha}P_{loss} \tag{2.6}$$

where ambient temperature is represented by $T_{ambient}$ and thermal resistance from ambient temperature to heatsink is represented by R_{ha}.

In [33], the author evaluates the failure rate of the circulator in stages. In this study, the reliability was evaluated in hours. In other words, the hourly failure rate evaluation unit was not divided by the operational phase. Therefore, the failure rate of converter can be calculated as:

$$\lambda = \prod_{PM} \prod_{process} \prod_{induced} (\gamma_{TH} \prod TH + \gamma_{TC} \prod TC + \gamma_{M} \prod M + \gamma_{RH} \prod RH) \tag{2.7}$$

where Π_{PM} is manufacturing factor reflecting the quality of the component, $\Pi_{process}$ is the factor that reflects the aging quality of the component during its life cycle, $\Pi_{induced}$ is the factor reflecting its overstress ability, λ_{M-RH} and λ_{TH-TC} are basic failure rates influenced by mechanical/humidity and factors temperature/thermal cycling, respectively, and $\gamma_{TH}, \gamma_{TC}, \gamma_{M}, \gamma_{RH}$ are the basic temperature (temperature, thermal cycling, mechanical factor and humidity).

Instead of using a constant ambient temperature, this model uses the real-time hourly ambient temperature to better calculate the hourly failure rate.

The main parameters for this model are shown below:

parameters	values
V_{IGBT}	1.54V
R_{IGBT}	$0.84\times10^{-3}\Omega$
f	3000Hz
E_{on}	0.50J
E_{off}	0.57J
V_{DC}	1100V
$V_{ref,IGBT}$	1700V
$I_{ref,IGBT}$	2400A
U_g	563.4V
V_{LL}	690V
V_{diode}	0.81V
R_{diode}	1.5Ω
E_{diode}	0.39J
U	690V
N_1	6
N_2	6
R_{ha}	0.454°C/W
Π_{PM}	0.16
$\Pi_{process}$	0.4
$\Pi_{induced}$	7.12
γ_{TH}	0.359
γ_{TC}	0.523
γ_M	0.9
γ_{RH}	0.028

Table 2-1 Main parameters of the converter real-time failure mo

2.3 Model Test

After building the real-time failure model, some work is done to test the model to see if the model is working well. First the relationship between the wind speed and wind farm output is given:

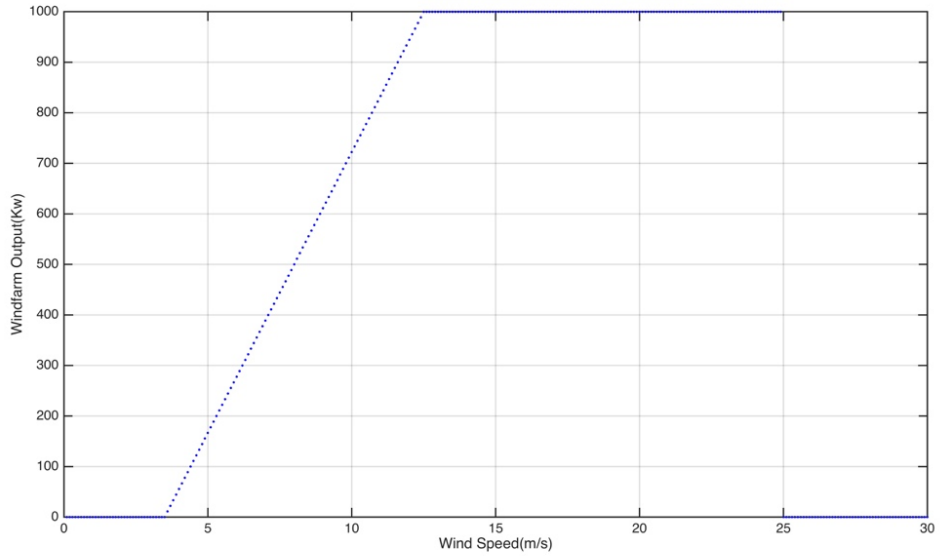

Figure 2-2 Relationship between wind speed and output

As shown above, the rated output for this wind turbine is 1000Kw. When the wind speed exceeds the rated wind speed V_r , the output remains a constant (1000Kw). When the wind speed is between V_c and V_r, the output increases linearly with increasing wind speed. The wind turbine stops working when the wind speed is over the cut-out speed or below the cut-in speed.

The real 24-hour temperature and wind speed in summer in Milwaukee is used to test the accuracy of this model, and they are shown below:

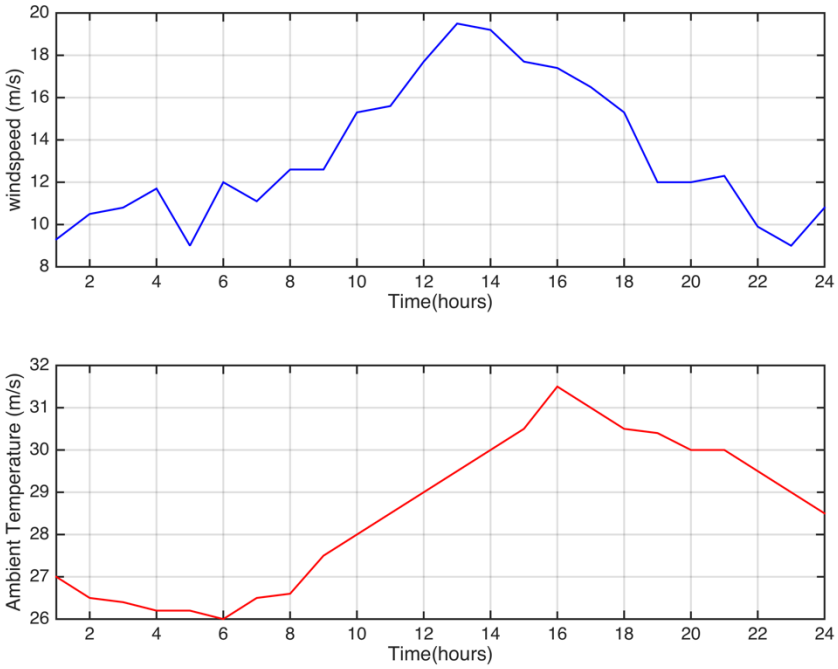

Figure 2-3 24-hour ambient temperature and wind speed in summer Milwaukee

As we can see from the figure above, the ambient temperature reaches its peak at 16:00 and the wind speed reached its peak at 13:00. It is easy to find that the wind speed fluctuates more than the temperature.

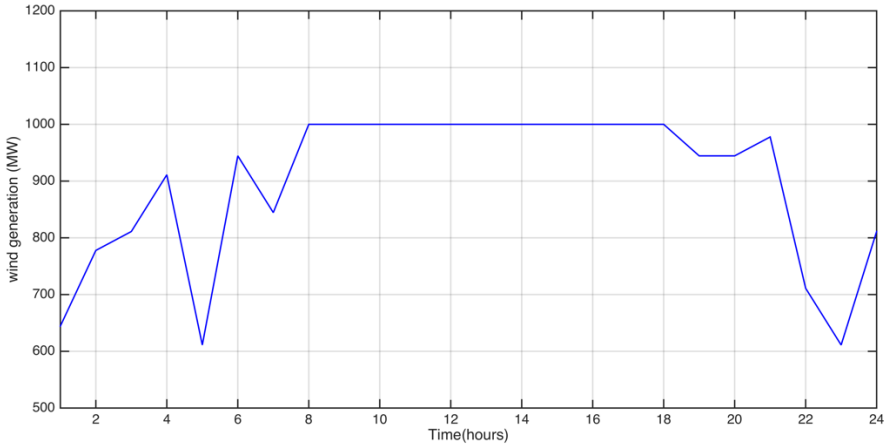

Figure 2-4 Real-time wind power output

As we can see from Figure 2-4 between 8:00 to 19:00, the wind power output remains 1000Kw, because the wind speed reaches the rated speed.

Based on the real-time data, the operating failure rate can be calculated below:

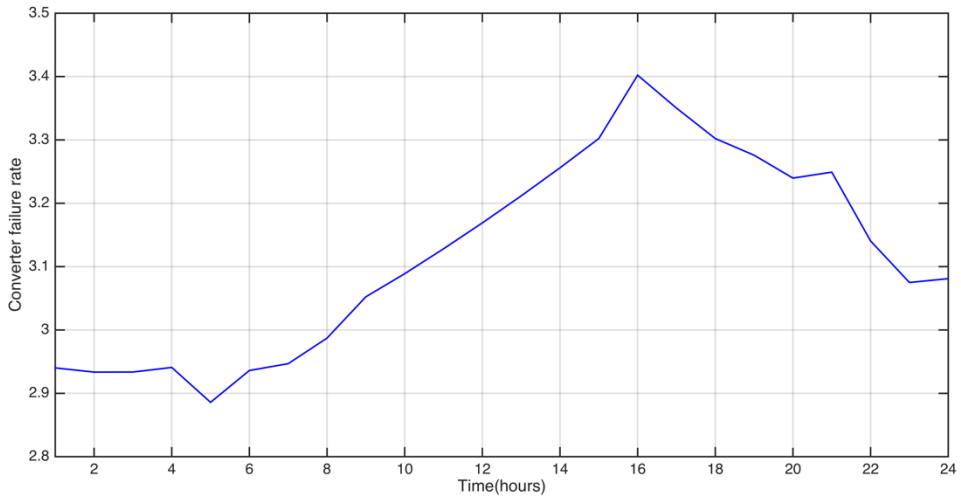

Figure 2-5 Real-time converter failure rate

As shown above, the failure rate reached a minimum of 2.88 failure per year at 5:00 and reached the highest point 3.40 at 16:00. Also the ambient temperature reached its peak at 16:00, and it is not difficult to find that the real-time failure rate curve is very similar to the ambient temperature curve, but is not exactly the same. Take the data at 20:00 and 21:00 as an example; the ambient temperature is both 30 Degrees Celsius, but the wind speed is 12 and 12.3 (m/s) respectively. As a consequence, the failure rate at 21:00 is higher than at 20:00 (3.24 to 3.24).

In order to demonstrate the superiority of the real-time failure rate model, the failure rate is compared with the following three cases. In these three cases we use the temperature and wind speed in Figure 2-3 to assume the rated wind farm output is 1 MW, other parameters are given in Table 2-1. In case 1, there is a converter with constant failure rate (3.11); in case 2, there is a converter with real-time failure rate considering the influence of wind speed only; in case 3, there is a converter with real-time failure rate considering the influence of wind speed and ambient temperature. As shown below, for Case 1 the failure rate is a fixed number; for Case 2 the failure rate fluctuates because of the hourly wind speed variation; and for Case 3 the curve fluctuates more violently and

has day and night characteristics. From 1:00 to 8:00 the failure is relatively low because of the low temperature at night, and from 11:00 to 20:00 the failure rate is higher because of the high ambient temperature in the day time.

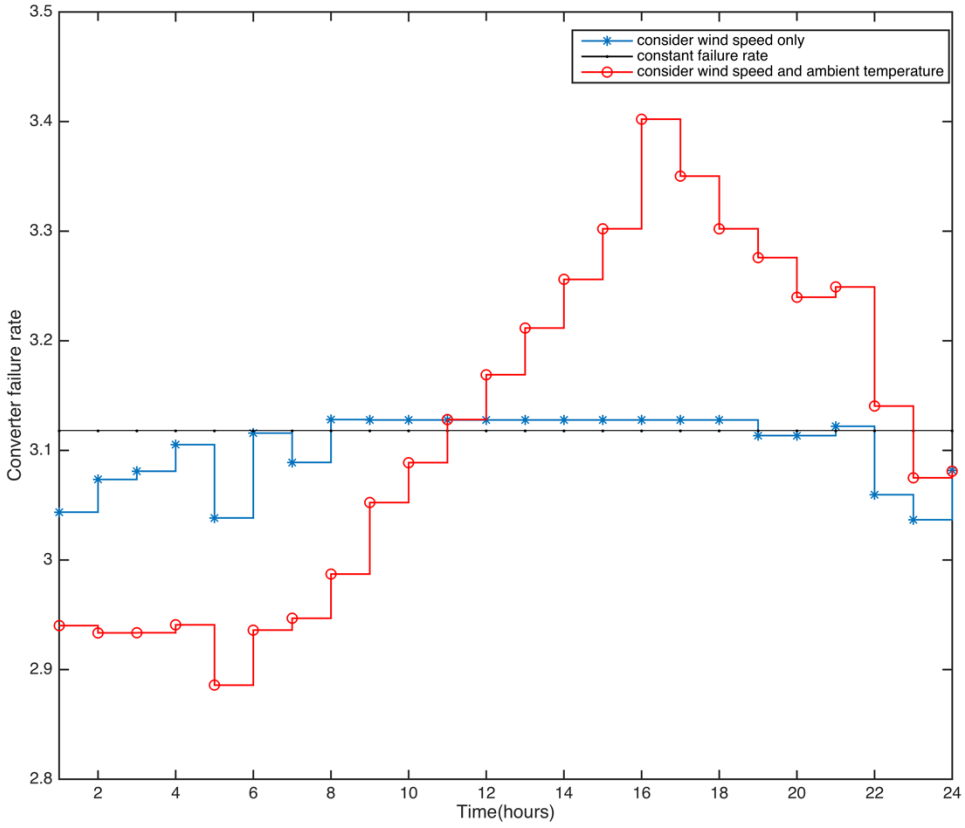

Figure 2-6 The compare of three failure rate

2.4 Conclusion and Future work

In this chapter a VSC real-time failure rate model is built and tested. For this model, first the hourly windfarm output is calculated from the real-time wind speed. Then the total power loss of the power electronics is calculated and the temperature rise over the VSC is also calculated, where the temperature rise caused by the ambient temperature is also considered. Finally, the VSC real-time failure rate can be calculated.

To test this model, the local temperature and wind speed are used, and the reliability index in different Cases is compared. The test results show that, with the real-time wind speed change, VSC failure rate will produce the corresponding change. The effect of ambient temperature on the failure rate of the converter is very significant in the stable operating environment. And the outage is more likely to happen during the daytime because of the high temperature. In general, this model can better reflect the impact of operating environment and operating status on VSC failure rate.

Future work can be focused on the following aspects: considering the impact of extreme weather on VSC failure rate; combining with wind speed and temperature forecast technology to study the failure rate prediction of the converter; the establishment of other power electronic equipment real-time failure rate model.

Chapter 3 A Transformer Real-time Failure Model

3.1 Introduction

Whether in HVAC or in HVDC systems, transformers are very important components. The reliability of the transformer directly affects the reliability of the entire power system. At present, large-capacity transformers mainly are oil-based. The insulation aging and mechanical strength loss of the transformer are mainly accelerated by overloading, and the aging process can increase the failure rate of the transformer, leading to frequent interruption and outage. The IEEE Guide [35] details the aging process of the transformer and its quantitative calculation. The figure below illustrates how the Hottest Spot Temperature (HST) accelerates its aging.

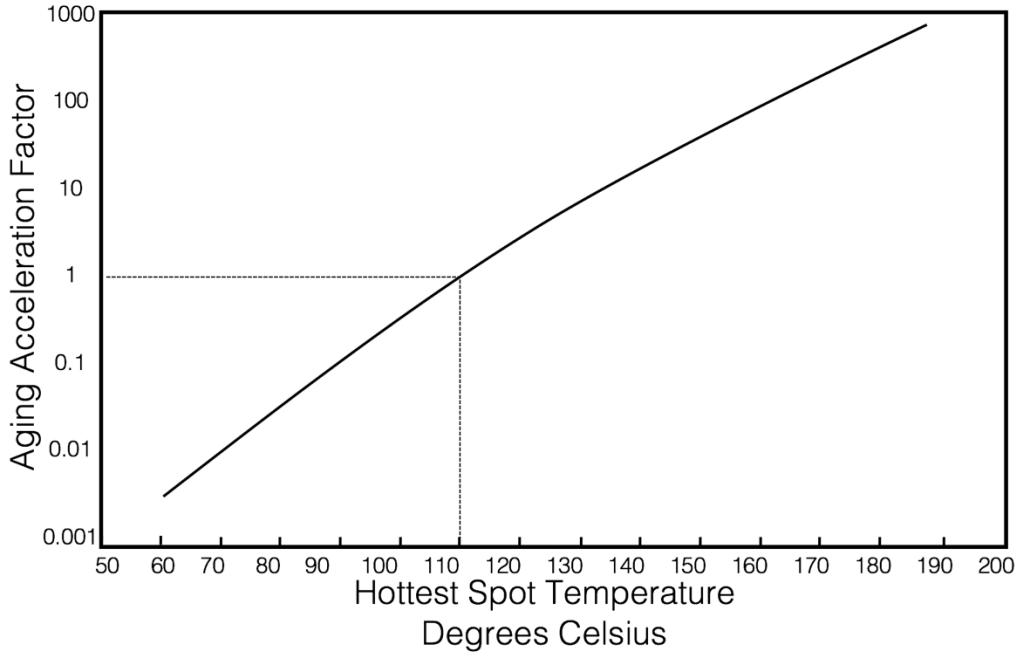

Figure 3-1 Aging acceleration factor (relative to 110 Celsius Degree)

The HST is the limiting temperature for a transformer's insulation. If the HST is over its limitation it will accelerate its aging and cause other problems. The Aging Accelerate Factor (AAF) it used to measure the impact of the aging process, and can be calculated below[35]:

$$F_{AA} = EXP^{\left(\frac{1500}{273+110} - \frac{1500}{\Theta H+273}\right)} \quad (3.1)$$

The reference HST ΘH is 110 ℃ for a 65 ℃ average winding rise transformer. If the HST is greater than the reference temperature, the F_{AA} has a value greater than 1. If it is less than 1, the HST is below the reference temperature.

Beside aging leading to transformer failure, overcurrent protection and operating environment will also cause transformer outage. In this chapter, a transformer real-time failure model considering aging failure caused by the mechanical strength loss, random failure based on weather condition and failure caused by overload protection is built and tested.

The remainder of this chapter is organized in the following way. The real-time transformer failure rate model is presented in section 3.2. The parameter setting and model test are presented in section 3.3. The summary of this chapter is given in section 3.4.

3.2 Model Establishment

The model diagram is shown below. The transformer real-time failure model consists mainly of three parts. The first part is the aging failure rate model. The main input of this sub-model is the real-time output of the windfarm and the ambient temperature to calculate the HST, and the HST is used to get the real-time aging failure. The second sub-model is the weather dependent model, in which the outage probability caused by the weather condition is calculated. The third sub-model is the current-dependent overload protection failure model, in which the outage probability caused by over current protection is studied. The total probability of outage is added together in the end.

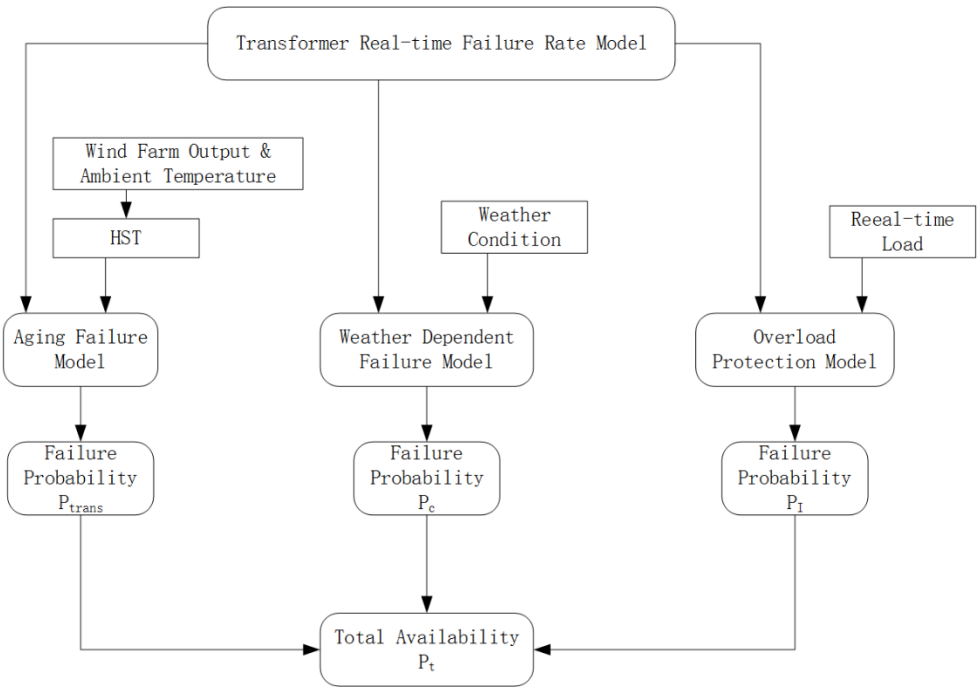

Figure 3-2 Transformer real-time failure rate model

3.2.1 Aging failure model

Aging failure is strongly related to the ambient temperature and loading of the transformer, which can be reflected by the winding HST. Before calculating the aging failure rate the hottest spot temperature should be calculated[36].

A. Hottest spot temperature calculation
First, top-oil temperature rise over ambient temperature $\Delta\theta_{TO}^{k}$ is calculated below:

$$\Delta\theta_{TO}^{k} = \Delta\theta_{TO}^{k-1} + (\Delta\theta_{TO,R} \times L_f(k) - \Delta\theta_{TO}^{k-1}) \times (1 - e^{-\frac{\Delta t}{\tau_{TO}}}) \tag{3.2}$$

$$L_f(k) = \left(\frac{(L(k)/L_r)^2 \times R_{ll} + 1}{R_{ll} + 1}\right)^{n1} \tag{3.3}$$

where $\Delta\theta_{TO}^{k}$ is the temperature increment of top-oil over the ambient temperature at hour k; $\Delta\theta_{TO,R}$ is the temperature increment of top-oil over ambient temperature when the transformer is working at rated load; τ_{TO} represents transformer thermal constant time; Δt is the length of time step k; L_f represents the transformer's loading factor, $L(k)$ is the actual load of the transformer at time k,

and L_r is the rated load of the transformer; R_{ll} is power loss ratio for the transformer at rated load to no load conditions; and $n1$ is the transformer's cooling class.

Second, the winding hottest spot temperature increment is calculated below:

$$\Delta\theta_H^k = \Delta\theta_H^{k-1} + (\Delta\theta_{H,R} \times L_f(k) - \Delta\theta_H^{k-1}) \times (1 - e^{-\frac{\Delta t}{\tau_w}}) \tag{3.4}$$

where the winding hottest spot temperature increment over top-oil temperature is represented by $\Delta\theta_H^k$; when the transformer is working at the rated load the hottest spot temperature increment is represented by $\Delta\theta_{H,R}$, and τ_w is transformer winding thermal constant time.

Then, the initial value for $\Delta\theta_{TO}$ and $\Delta\theta_H$ should be calculated:

$$\Delta\theta_{TO}^0 = \Delta\theta_{TO,R} \times L_f(0) \tag{3.5}$$

$$\Delta\theta_H^0 = \Delta\theta_{H,R} \times L_f(0) \tag{3.6}$$

Finally, the winding hottest spot temperature θ_H at hour *k* can be calculated as follows:

$$\theta_H^k = \theta_{AT}^{\square} + \theta_{TO}^k + \theta_H^k \tag{3.7}$$

where the ambient temperature can be represented by θ_{AT}^k.

B. Failure rate calculation

Since the dielectric strength of the conductor insulation decreases with the increment of the running time, the failure due to aging is mainly caused by the loss of the mechanical strength of the insulation [37]. This is an irreversible and cumulative process. Weibull distribution is the major method to describe the probability of transformer aging failure[19]. The failure of aging in these studies is considered to be an operating condition independent failure. In reality, the aging failure actually depends on the transformer's thermal conditions. As discussed in chapter 3.1, the relationship between HST and aging acceleration factor was already studied. Thus, the aging effects of HST are usually considered in aging studies.

First, a time period T can be divided into small time intervals $t1, t2, \ldots tk, \ldots$, and the insulation life loss during time interval tk can be calculated below[38]:

$$T_{loss} = t_k \times e^{\left(\frac{15000}{\theta_0+273} - \frac{15000}{\theta_H^k+273}\right)} \tag{3.8}$$

θ_0 is the reference temperature (110 ° C for 65 ° C average winding rise).

Then, the aging loss during time period T is calculated:

$$T_{loss,total} = \sum_{K=1}^{N} t_k \times e^{\left(\frac{15000}{\theta_0+273} - \frac{15000}{\theta_H^k+273}\right)} \tag{3.9}$$

Last, the aging failure probability of a transformer based on the HST can be computed:

$$P_{af} = 1 - e^{\left(\frac{T_{loss,total}}{\frac{15000}{Ce^{\theta_0+273}}}\right)^{\beta} - \left(\frac{T_{loss,total}+\Delta t_e}{\frac{15000}{Ce^{\theta_0+273}}}\right)^{\beta}} \tag{3.10}$$

where Δt_e is the equivalent operation time and C and β are end-of-life failure constant value[35], [39].

In addition to the aging failure, the random failure of different components is also taken into account and they are independent of each other. Given an assumed random failure probability P_{random}, the transformer failure probability can be calculated below:

$$P_{trans} = 1 - (1 - P_{random}) \times (1 - P_{af}) \tag{3.11}$$

3.2.2 Weather dependent failure model

Due to other factors such as size and land area, most transformers in power transmission systems are exposed to different weather conditions such as winds, typhoons, heavy rains, snow and ice. Even with the establishment of the oversea transformer substation, the operation of the converter station will be affected by the weather conditions. The failure rate of the transformer exposed to

the weather is much greater than in the general case [15]. In this section, a simplified weather-dependent failure rate model is used. The failure rate is as follows:

$$\lambda_c(\omega) = \begin{cases} \bar{\lambda}\frac{N+S}{N}(1-F), & \omega = 0 \\ \bar{\lambda}\frac{N+S}{N}F, & \omega = 1 \end{cases} \tag{3.12}$$

where N represents the duration of normal weather scenario, S represents the duration of adverse weather scenario, F is the failure probability in adverse weather, ω is transformer operating weather condition (in normal weather ω is 0, and ω is 1 in adverse weather).

The probability is illustrated below:

$$P_c = 1 - e^{-\lambda_c(\omega)\Delta t} \tag{3.13}$$

3.2.3 Overload protection model

Because the overload protection can also lead to the transformer outage, a current-dependent overload failure model is used in this section. There are several reasons for the current mismatch of a transformer [40]. There are uncertainties for outages due to the trip of breakers when the current is around the pickup value. Usually we used the standard deviation to describe the failure probability. I_{pick} is the relay pickup value, the range is $\left[I_{pe}(1-\varepsilon_1),\ I_{pe}(1+\varepsilon_1)\right]$ and its probability density is shown as follow:

$$P_{protection}(I) = \begin{cases} if: I < I_{pe}(1-\varepsilon_1) \\ P_{unrequired}, \\ if: I_{pe}(1-\varepsilon_1) < I < I_{pe}(1+\varepsilon_1) \\ P_{required}\int_{I_{pe}(1-\varepsilon_1)}^{I} f\left(I_{pick}\right) dI_{pick} + \\ P_{unrequired}\int_{I}^{I_{pe}(1+\varepsilon_1)} f\left(I_{pick}\right) dI_{pick} \\ if: \geq I_{pe}(1+\varepsilon_1) \\ P_{required}, \end{cases} \tag{3.14}$$

$P_{protection}(I)$ represents the transformer protection failure probability at current I; when the overload protection is not activated the failure probability is $P_{unrequired}$; when the overload protection is activated the failure probability is $P_{required}$; I_{pick} represents the protection relay pick-up current; I_{pe} represents the expectation value of I_{pick}; $\varepsilon_1$is current mismatch percentage error; the probability density function is represented by $f(I_{pick})$. The function is formulated as follows:

$$f(I_{pick}) = \begin{cases} 0 & I_{pick} < I_{pe}(1-\varepsilon_1)\ or\ I_{pick} > I_{pe}(1+\varepsilon_1) \\ \frac{1}{\alpha_1 \sigma \sqrt{2\pi}} e^{-(\frac{(I_{pick}-I_{pe})^2}{2\sigma^2})} & I_{pe}(1-\varepsilon_1) < I_{pick} < I_{pe}(1+\varepsilon_1) \end{cases} \quad (3.15)$$

$$\alpha_1 = \phi\left(\frac{\varepsilon I_{pe}}{\sigma}\right) - \phi\left(\frac{-\varepsilon I_{pe}}{\sigma}\right) \quad (3.16)$$

where σ^2 is the variance of I_{pick}, and ϕ is the cumulative distribution function.

Because these three outage models are different and independent, the total real-time failure probability of a transformer can be calculated by condition probability concept as follows:

$$P_t = 1 - (1 - P_{trans}) \times (1 - P_c) \times (1 - P_I) \quad (3.17)$$

3.3 Model test

After building the transformer real-time failure model, some work is done to test the model to see if the model works well. First the aging failure sub-model is built.

The main parameters for this model are shown below:

parameters	values
$\Delta\theta_{T0,R}$	36.0℃
$\Delta\theta_{H,R}$	28.6℃
R	4.87
τ_{T0}	3.5 h
τ_w	3 min
m	1.0
n	1.0

β	5.9
B	15000
C	1.903×10^{-12}

Table 3-1 Main parameters of the aging failure model

parameters	values
N	200 h
S	2 h
F	0.6
$\bar{\lambda}$	0.02 $year^{-12}$

Table 3-2 Main parameters of the weather dependent failure model

parameters	values
I_{P0}	1.5
σ	0.045
ε	9%
P_w	0
P_Z	1

Table 3-3 Main parameters of the overload protection failure model

3.3.1Aging failure model test

To test this model, the same load and weather data is used as it was in the converter model. First the HST is calculated:

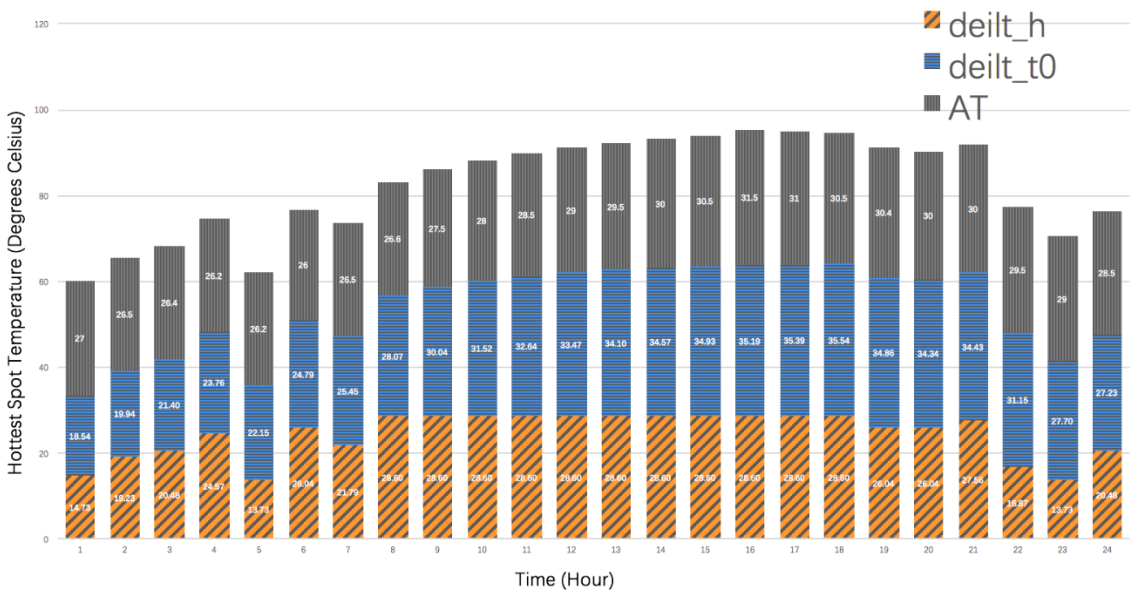

Figure 3-3 Hottest spot temperature calculation

In the figure above, the winding HST increment over top-oil temperature $\Delta\theta_H^k$ and top-oil increment over ambient temperature $\Delta\theta_{TO}^k$ are calculated, and the ambient temperature is also given. The winding HST is the sum of their three values. It is not difficult to find that the other two increments are less volatile than ambient temperature. Under the condition that the operating load is relatively stable, the winding HST is mainly affected by ambient temperature.

In order to illustrate the impact of the aging process on the transformer failure rate, the aging process of the transformer is independently tested：

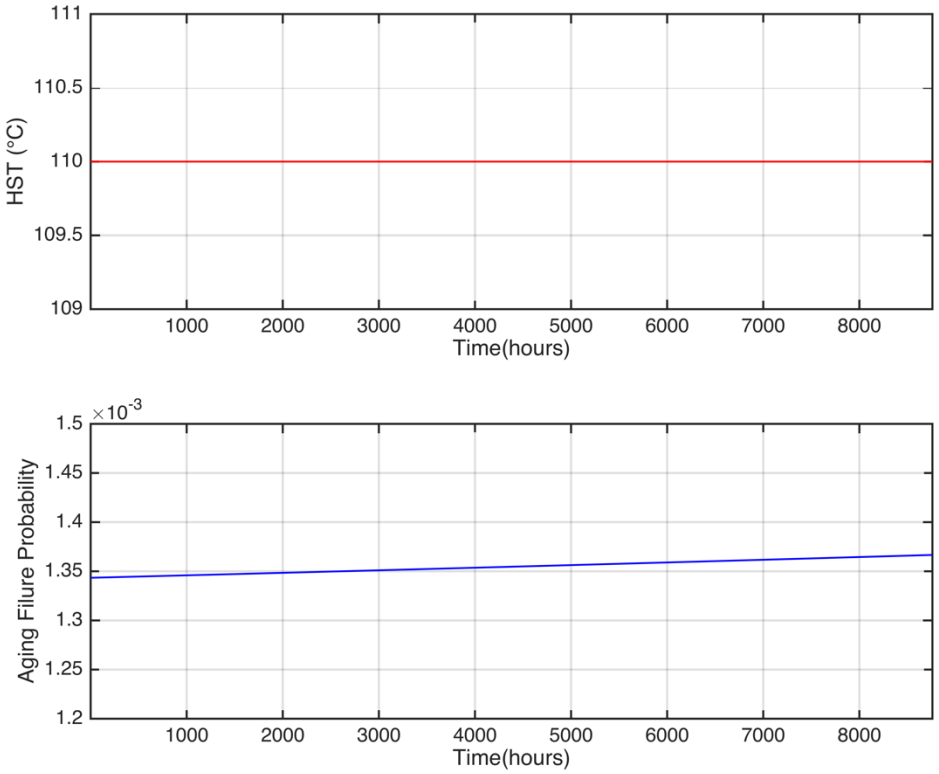

Figure 3-4 Transformer failure caused by aging

In this test, we set a transformer operating under full load and at 25 Degrees Celsius for 20 years. Figure 3-4 shows the HST and aging failure rate in the 21st year. Because the load and the temperature is fixed, the HST remains a constant. At the same time, the failure rate increases slowly over time. Thus, the aging failure is correct and it cannot be ignored.

3.3.2Overload protection model test

To test the overload protection model, the probability density is calculated below:

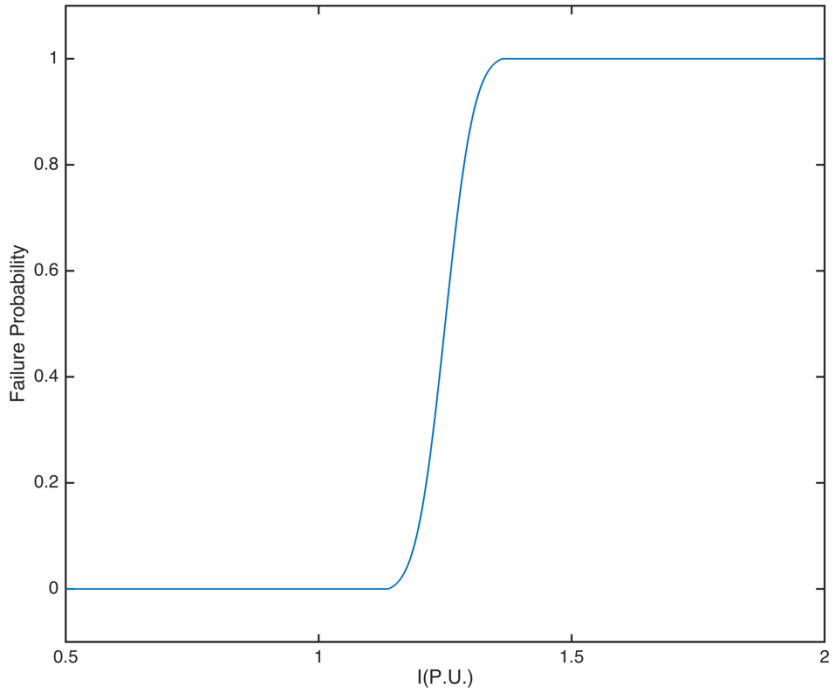

Figure 3-5 Probability density for overload protection failure

In the figure above we can find that, when the current is below $I_{p0}(1-\varepsilon)$ the failure probability is 0, when the current is over $I_{p0}(1+\varepsilon)$ the failure probability is 1, and when the current is I_{p0} the outage probability is 0.5. By setting the valve of I_{p0} we can adjust the protection.

3.3.3 Total failure rate probability test

The 24-hour transformer failure is calculated based on the work above. In this calculation, we set a transformer operating under full load and at 25 Degrees Celsius for 20 years. And we assumed the weather condition is good in this 24-hour period.

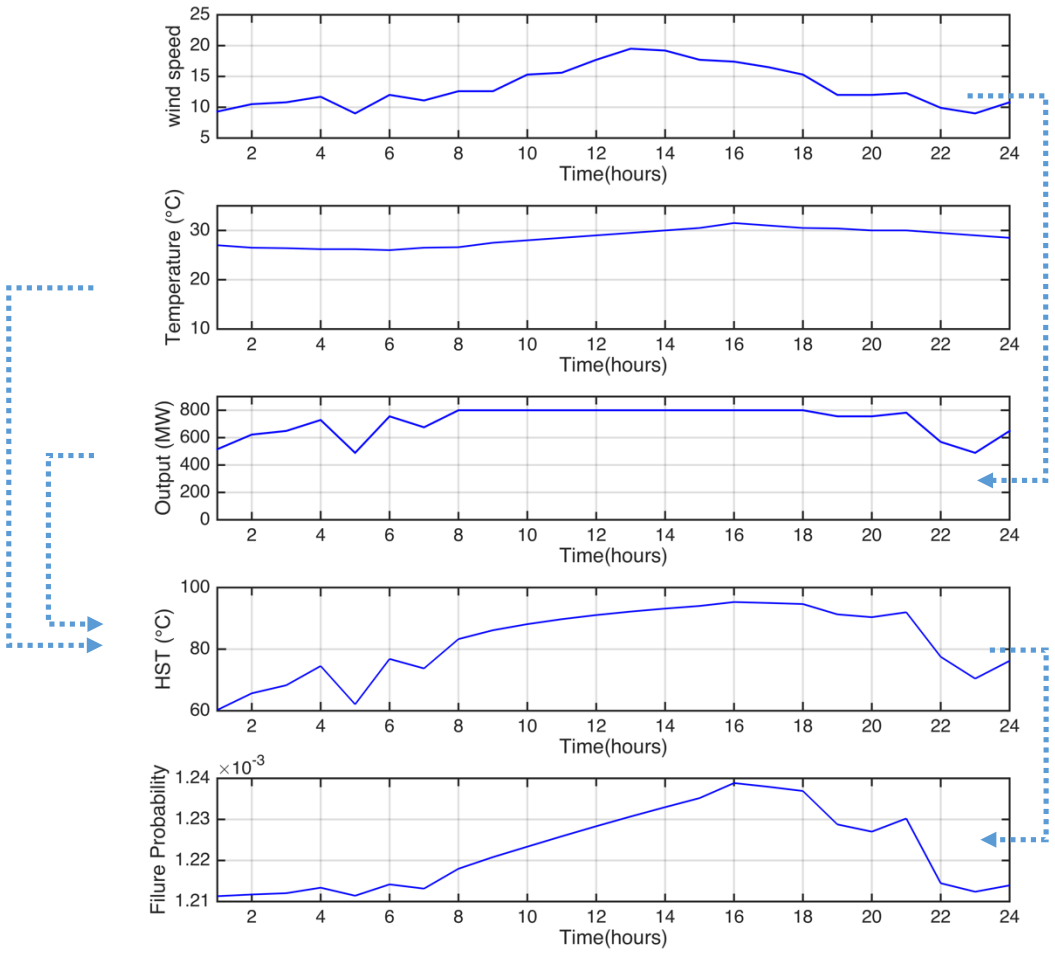

Figure 3-6 Transformer failure probability calculation

As we can see above, the wind speed directly determines the output of the wind farm. The output and the ambient temperature are the two main factors for the HST, and the trend of HST changes can be seen as a superposition of both of them. The failure probability of this transformer in 24hours reaches its peak at 16:00 and the peak of HST is also at 16:00. This is because the aging failure is the main factor in normal operating conditions.

To compare the influence of these three sub-models, the tests below are done. The same 24-hour ambient temperature and wind speed data is used. In case 1, the transformer has operated at 110 Degrees Celsius for 5 years and the weather condition is normal weather. In case 2, the transformer

has operated at 110 Degrees Celsius for 5 years and the weather condition is adverse weather. In case 3, the transformer has operated at 110 Degrees Celsius for 30 years and the weather condition is normal weather. In case 4, the transformer has operated at 110 Degrees Celsius for 30 years and the weather condition is adverse weather.

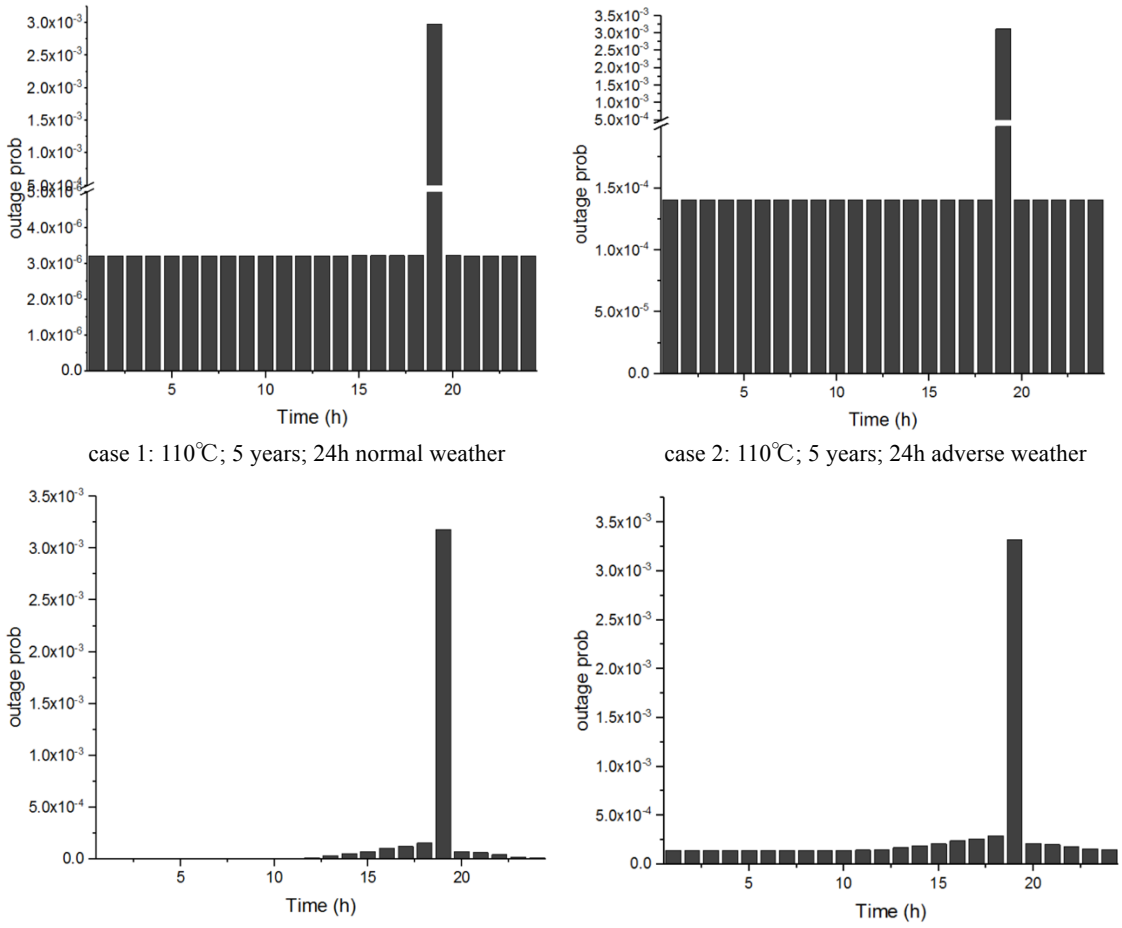

Figure 3-7 Four cases for transformer real-time failure model test

The figure above illustrates the outage probability of the 4 cases. The sharp increase at 19:00 is because of the over current protection. When comparing case 1 with case 2 and case 3 with case 4, we can find that the weather condition can affect a transformer's outage probability evidently. When operating in adverse weather, the outage probability will increase. When comparing case 1

with case 3 and case 2 with case 4, we can find that, in case 1 and case 2 the transformer is in normal operating state, in case 3 and case 4 the transformer is in wear-out operating state. In the normal operating stage, the weather condition, HST, and overcurrent protection have a common impact on the outage probability. But in the wear-out stage, the HST is the main factor for this model.

3.4 Conclusions and Future Work

In this chapter a transformer real-time outage probability model is built and tested. For this model, first the HST is calculated based on the wind farm real-time output and hourly ambient temperature, and an aging failure model is built. Second, an overcurrent protection failure model is established to calculate the outage probability caused by the over current. Then, a weather-dependent failure model is built in order to take climate factors into account. Finally, the three sub-models are combined to get the final transformer real-time outage probability model.

To test this model, the local temperature and wind speed are used, the hourly HST, aging process, overload protection curve and real-time failure probability are calculated. Four cases are studied to compare these three sub-models. The test results show that, each sub-model can accurately reflect the real-time outage probability of the transformer, and with the aging process intensified, the degree of impact will change. Even if the transformer is operating in the normal condition, the aging process will increase its outage probability slowly.

Future work can be focused on the following aspects: considering more weather conditions for the weather-dependent failure model; combining wind speed and temperature forecast technology to

study the outage probability prediction of the transformer; adjusting the structure of the model according to the structure and function of the transformer.

Chapter 4 Case Study

4.1 Introduction

In this chapter a radial VSC-HVDC transmission system and a regional VSC-HVDC transmission system for offshore wind energy are studied. First, the explanation of each component in the system and their reliability parameters are studied in reference [8]. Due to the special structure of offshore wind power; in this paper, the parameters for the same equipment were distinguished by onshore and offshore. Then, by using the minimum cut set method, topologies of these two system are simplified and the reliability index is calculated.

Before the case study, two indicators are illustrated. First the availability of each component in the system can be computed from the formula below:

$$A = \frac{MTTF}{MTTF+MTTR} \tag{4.1}$$

for a specific component, A is availability, $MTTF$ represents mean time to failure and $MTTR$ represents mean time to repair. Availability can also be calculated by failure rate λ and repair rate μ:

$$A = \frac{\mu}{\lambda+\mu} \tag{4.2}$$

For the system, energy availability is defined as the maximum amount of energy which could have been transmitted.

The remainder of this chapter is organized in the following way. The reliability parameters for each

component are studied in section 4.2. The case study for a radial VSC-HVDC transmission system is presented in section 4.3. The case study for a regional VSC-HVDC transmission system is presented in section 4.4. The summary of this chapter is given in section 4.5.

4.2 Component reliability and parameters

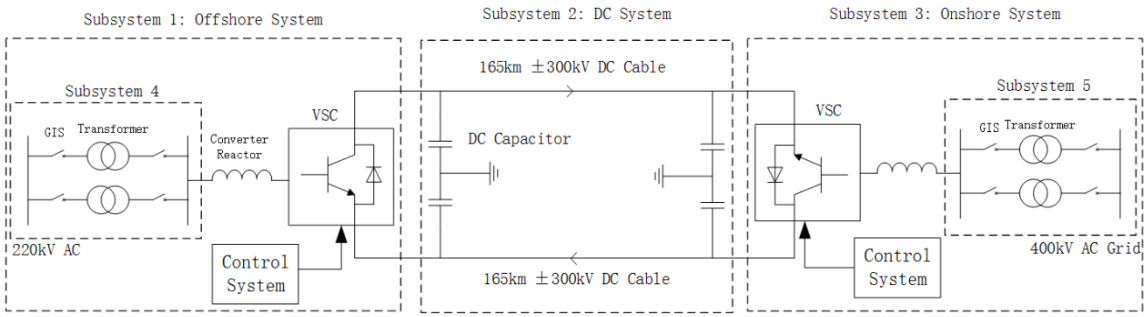

Figure 4-1 Radial VCS-HVDC transmission system

A point to point VSC-HVDC scheme is shown above. It can be divided into three subsystems (offshore system, DC system, and onshore system) and a transformer subsystem, which consists of transformer and GIS in both offshore and onshore systems. For the converter, the failure caused by control system is also considered. The DC system consists of an offshore DC switchyard, DC cables, and an onshore DC switchyard. The fixed reliability indices are cited from reference [8].

4.2.1 Converter and Converter Reactor

For the converter, the real-time failure rate can be calculated by the model in chapter 2. But to calculate the availability of the converter, the repair time is also required. Because offshore wind power is far from land and the environment is complex, the repair time for offshore converters and onshore converters must be different. According to reference [8] the repair time for offshore converters is 15 hours, and the repair time for onshore converters is 6 hours.

The converter reactor is connected in series with each arm of the converter. The reliability indices were cited in reference [8] from DNV and they are given below:

Component	MTTF(year)	MTTR(hour)	Availability
Onshore Converter Reactor	7	24	0.99961
Offshore Converter Reactor	7	192	0.99688

Table 4-1 Reliability indices for converter reactor

The MTTR for offshore is bigger because of the difficulty for oversea repair. Also the availability for converter control systems is given.

Component	MTTF(year)	MTTR(hour)	Availability
Onshore Control System	1.6	3	0.99979
Offshore Control System	1.6	17	0.99879

Table 4-2 Reliability indices for control system

4.2.2 Transformer and GIS

The real-time availability for the transformer can be calculated by using the model in chapter 3. To distinguish between offshore transformers and onshore transformers we can adjust the value of the P_{random} in 3.2.1

$$P_t = 1 - (1 - P_{trans}) \times (1 - P_c) \times (1 - P_l) \tag{4.3}$$

For an offshore transformer P_{random} is settled to be 0.00181; for an onshore transformer P_{random} is settled to be 0.00121.

In a VSC-HVDC switchyard the major components are switchgear, measurement equipment, line reactors and capacitor banks. Because the GIS switchyard is a closed system, the availability is not

largely dependent on the environment; the availability for both sides is settled to be 0.99992.

4.2.3 DC System

The estimated reliability indices for the DC switchyard are provided below:

Component	MTTF(year)	MTTR(hour)	Availability
Onshore DC Switchyard	4.02	26.06	0.99926
Offshore DC Switchyard	4.02	98.06	0.99723

Table 4-3 Reliability indices for DC switchyard

Based on the DNV value the failure rate for a DC cable is 0.07 failures per year per 100 km. And the repair time is 60 days.

Component	Failure rate (occ/yr/100km)	Length(km)	MTTF(year)	MTTR(hour)	Availability
DC Cable	0.07	165	8.4936	1440	0.98101

Table 4-4 Reliability indices for submarine cable

The availability indexes for all the components are shown below:

Component	Offshore	Onshore
GIS	0.99992	0.99992
Transformer real-time	**0.99819 Based**	**0.99879 Based**
Converter reactor	0.99961	0.99688
Converter real-time	**15 h repair time**	**6 h repair time**
Control system	0.99879	0.99979
DC switchyard	0.99723	0.99926

DC cable	0.07(0cc/yr/100km)	MTTR1440

Table 4-5 Reliability indices summary

4.3 Case 1: Radial HVDC Transmission System

In this case, based on the wind speed and ambient temperature from a given 24-hour period, the energy availability for a radial system was calculated. The radial VSC-HVDC transmission is given below, and the reliability indices for components have already been given in 4.2

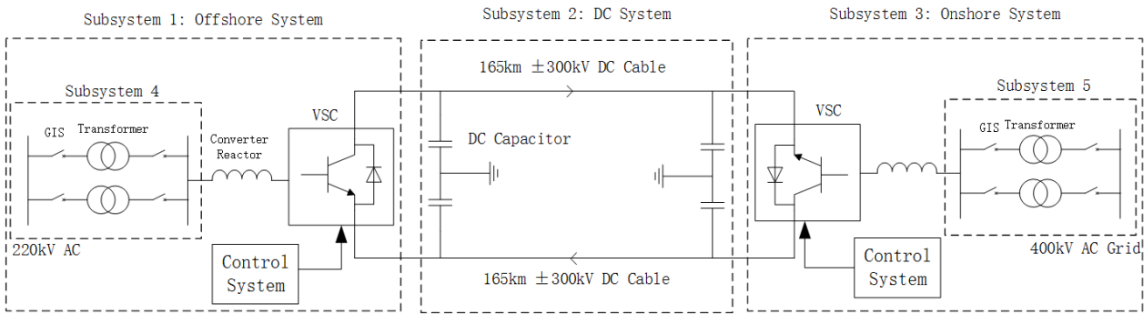

Figure 4-2 Radial VCS-HVDC transmission system

First, by using the concept of minimum cut set, this system can be simplified to the figure below:

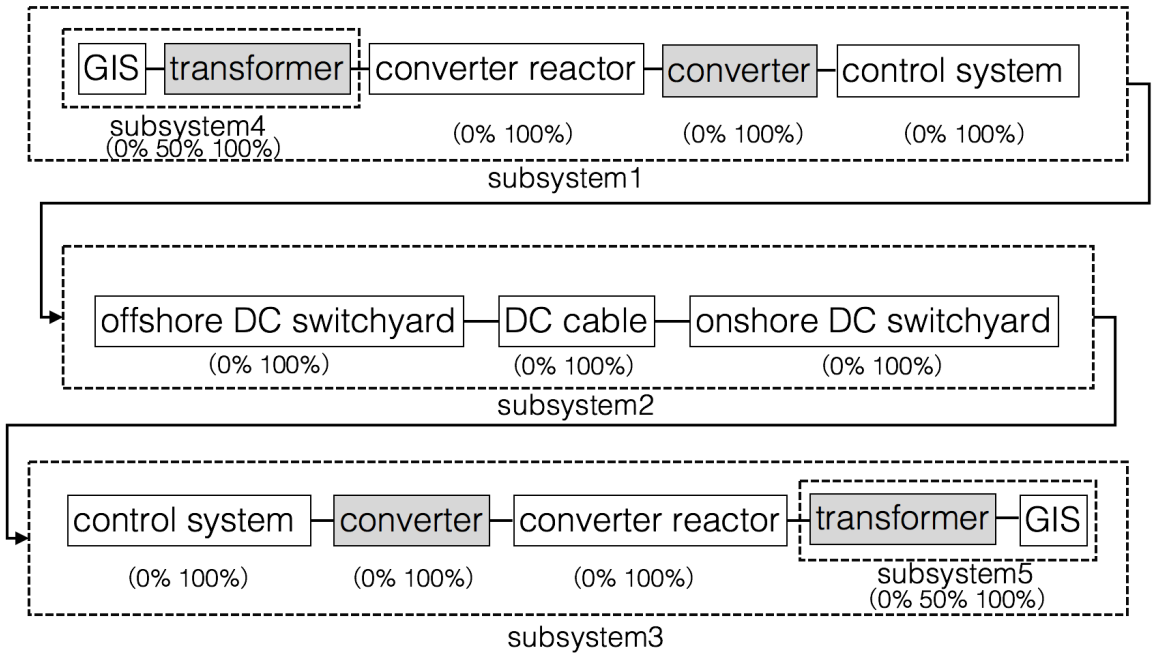

Figure 4-3 Simplification for radial VCS-HVDC transmission system

In this figure, all the components are in series, and all the components except the transformer system are two-state models. For the two parallel transformers, the operating state can be divided into three states (0%, 50%, 100%)

Next, the energy availability for this radial system was calculated. The 24-hour wind speed and ambient temperature for Milwaukee in 2010 were used and given below:

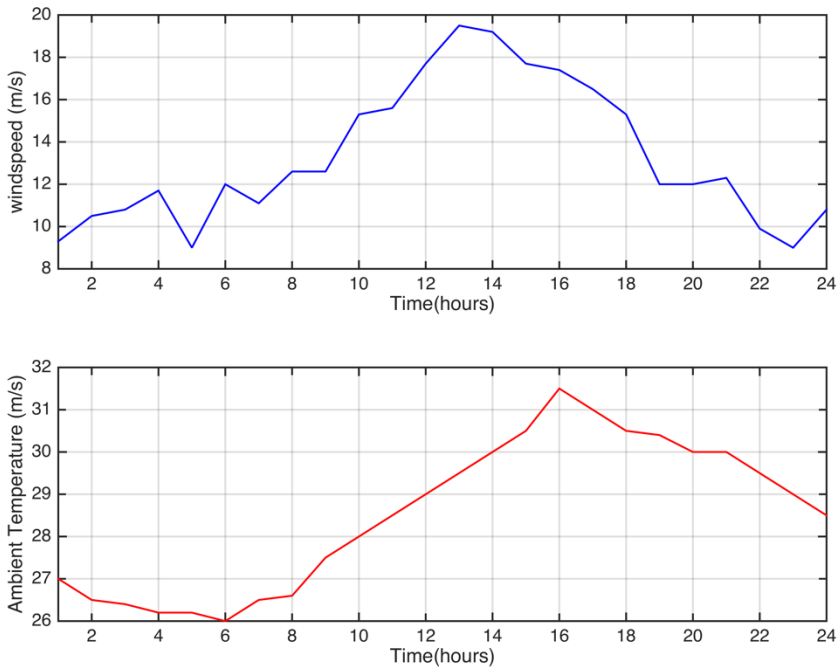

Figure 4-4 24-hour ambient temperature and wind speed in summer Milwaukee

The curve above is ambient temperature and the curve below is the wind speed. We can find that the peak of the wind speed is at 13:00 and the peak of the ambient temperature is at 16:00.

The real-time availability for the converters is calculated below:

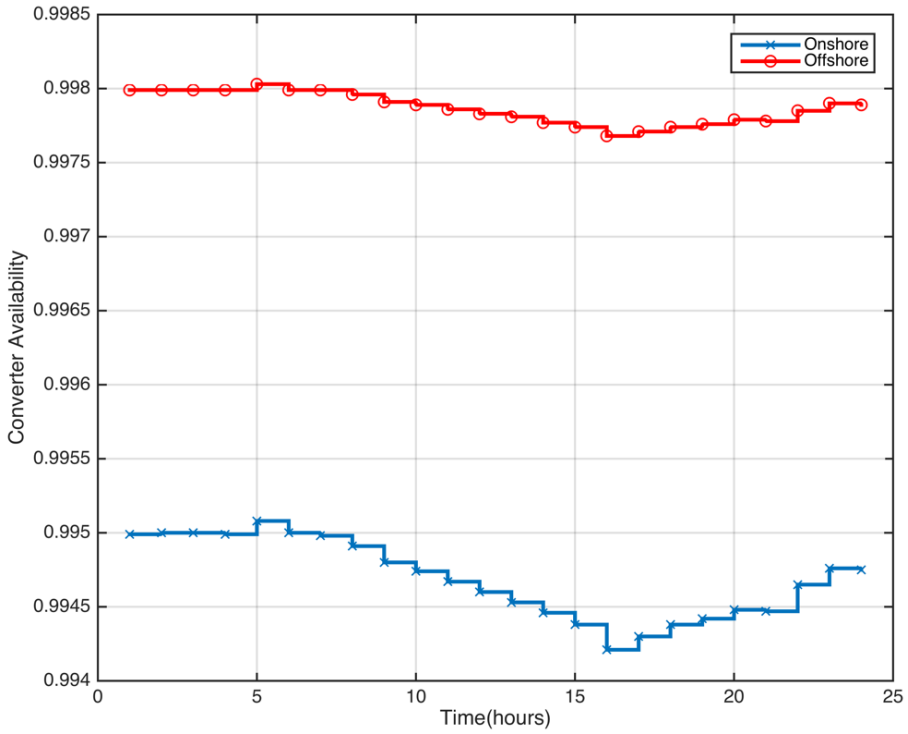

Figure 4-5 Availability for onshore and offshore converters

From the curves above we can find that, the availability for the onshore converter is higher. This is because of the shorter repair time. The two lines have the same trend, and both reach their lowest point at 16:00. This is because of the high ambient temperature at that time.

The real-time availability for the transformers is calculated below:

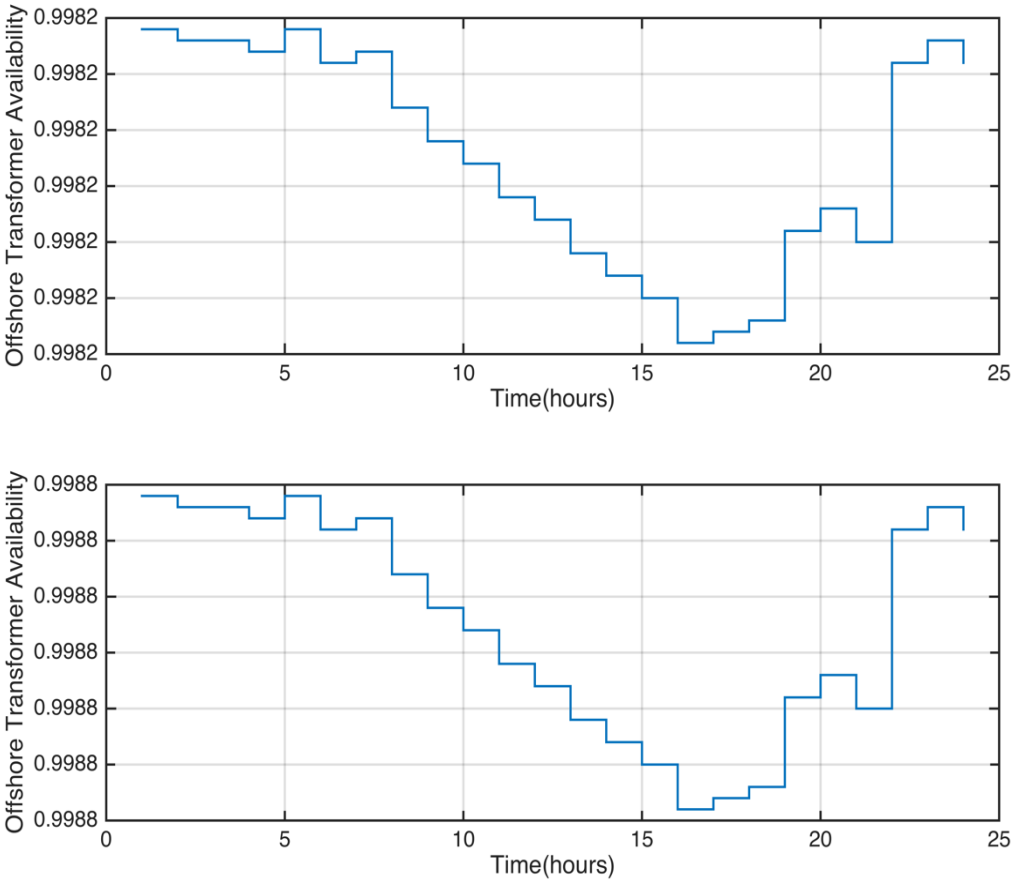

Figure 4-6 Availability for onshore and offshore transformers

From the graphs above we can find that the availability for the onshore transformer is higher. This is because we adjust the P_{random}. The two lines have the same trend, and both reach their lowest point at 16:00. This is because of the high ambient temperature at that time.

The hourly availability of these three subsystems is then calculated.

System	System1			System3			System2	
Time	100%	50%	0	100%	50%	0	100%	0%
1	0.98678469	0.00358123	0.00963409	0.99465834	0.0024126	0.00292906	0.97757	0.02243
2	0.98679505	0.00358207	0.00962288	0.99466205	0.00241342	0.00292454	0.97757	0.02243
3	0.98679423	0.0035827	0.00962308	0.99466133	0.00241405	0.00292462	0.97757	0.02243
4	0.98677942	0.00358529	0.00963529	0.99465374	0.0024167	0.00292955	0.97757	0.02243
5	0.98687584	0.00358177	0.00954239	0.99469507	0.0024129	0.00289203	0.97757	0.02243
6	0.9867859	0.00358691	0.00962719	0.99465541	0.00241831	0.00292628	0.97757	0.02243
7	0.98676987	0.0035848	0.00964533	0.99465016	0.00241624	0.00293361	0.97757	0.02243
8	0.98669244	0.00359411	0.00971345	0.99461307	0.0024258	0.00296113	0.97757	0.02243
9	0.98657723	0.00359928	0.00982349	0.9945631	0.00243132	0.00300558	0.97757	0.02243
10	0.98651099	0.00360408	0.00988493	0.99453327	0.00243632	0.00303041	0.97757	0.02243
11	0.98643999	0.00360881	0.00995119	0.99450154	0.00244127	0.00305719	0.97757	0.02243
12	0.98636641	0.0036134	0.01002019	0.99446884	0.00244608	0.00308507	0.97757	0.02243
13	0.98629017	0.0036178	0.01009203	0.99443518	0.00245071	0.00311411	0.97757	0.02243
14	0.98621118	0.00362201	0.01016681	0.9944005	0.00245517	0.00314433	0.97757	0.02243
15	0.98612928	0.00362608	0.01024464	0.99436472	0.00245948	0.00317579	0.97757	0.02243
16	0.98595417	0.00363268	0.01041315	0.99428948	0.0024666	0.00324392	0.97757	0.02243
17	0.98604315	0.00363121	0.01032564	0.99432658	0.00246487	0.00320854	0.97757	0.02243
18	0.98612587	0.00362948	0.01024465	0.99436129	0.00246291	0.0031758	0.97757	0.02243
19	0.98618612	0.00361361	0.01020027	0.99439536	0.00244678	0.00315785	0.97757	0.02243
20	0.98625027	0.00361036	0.01013937	0.99442343	0.00244334	0.00313324	0.97757	0.02243
21	0.98622819	0.00361662	0.01015518	0.99441067	0.0024497	0.00313963	0.97757	0.02243
22	0.98644185	0.00358622	0.00997192	0.99451591	0.00241854	0.00306556	0.97757	0.02243
23	0.98655594	0.00358253	0.00986153	0.99456453	0.00241452	0.00302095	0.97757	0.02243
24	0.98654276	0.00358555	0.00987169	0.99455735	0.00241759	0.00302505	0.97757	0.02243

Table 4-6 Hourly availability for three subsystems

In the figure above we can find that although system 1 and system 3 have the same structure, the availability for system 3 is higher. This is because system 3 is an onshore system. Take the availability at 16:00 as an example; for system 1, the system will operate at full capacity approximately 98.6% of the time, half capacity 0.36% of the time, and zero capacity 1.04% of the time.

The availability for the whole system was then calculated. First the availability in each stage is given.

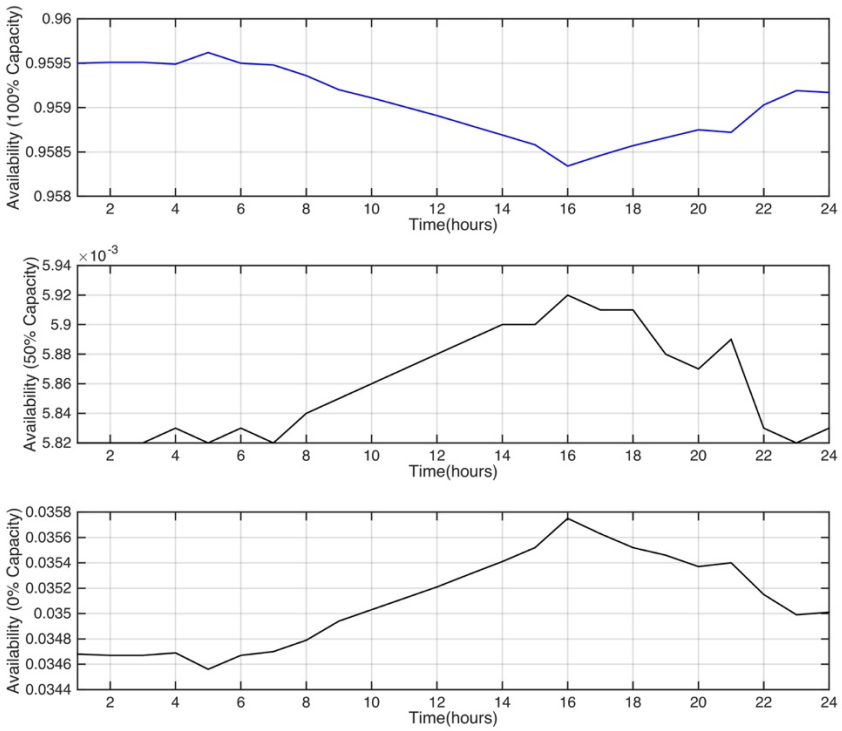

Figure 4-7 System availability for radial system

As we can see above, the availability for 100% capacity stage is lowest at 16:00. This is because of the high ambient temperature and high wind speed. Conversely, the reliability is high at mid-night because of the low temperature and wind speed.

Take the availability at 16:00 as an example; for this point to point transmission system, the system will operate at full capacity approximately 95.8% of the time, half capacity 0.59% of the time, and zero capacity 3.57% of the time. And the total energy availability is 96.13%.

The specific value is given below:

Time	Availability 100%	Availability 50%	Availability 0	Energy Availability
1	0.95949827	0.00581796	0.03468377	0.96240725
2	0.95951192	0.00581961	0.03466847	0.96242172
3	0.95951043	0.00582083	0.03466874	0.96242085
4	0.95948871	0.00582587	0.03468542	0.96240165
5	0.95962234	0.00581912	0.03455854	0.9625319
6	0.95949663	0.00582902	0.03467435	0.96241114
7	0.95947596	0.00582491	0.03469913	0.96238842
8	0.9593649	0.00584293	0.03479217	0.96228637
9	0.95920469	0.00585286	0.03494245	0.96213112
10	0.95911152	0.00586211	0.03502636	0.96204258
11	0.9590119	0.00587124	0.03511686	0.96194752
12	0.95890884	0.00588007	0.0352111	0.96184887
13	0.95880227	0.00588853	0.0353092	0.96174653
14	0.95869203	0.00589664	0.03541132	0.96164036
15	0.95857793	0.00590446	0.03551761	0.96153016
16	0.9583352	0.00591708	0.03574772	0.96129374
17	0.95845745	0.00591433	0.03562823	0.96141461
18	0.9585713	0.00591107	0.03551763	0.96152684
19	0.95866272	0.00588026	0.03545701	0.96160286
20	0.95875214	0.00587401	0.03537385	0.96168915
21	0.95871838	0.00588617	0.03539544	0.96166147
22	0.95902756	0.00582727	0.03514517	0.9619412
23	0.95918538	0.00582022	0.0349944	0.96209549
24	0.95916564	0.00582609	0.03500828	0.96207868

Table 4-7 Hourly availability for three subsystems

Finally, the energy availability is calculated with the processes above.

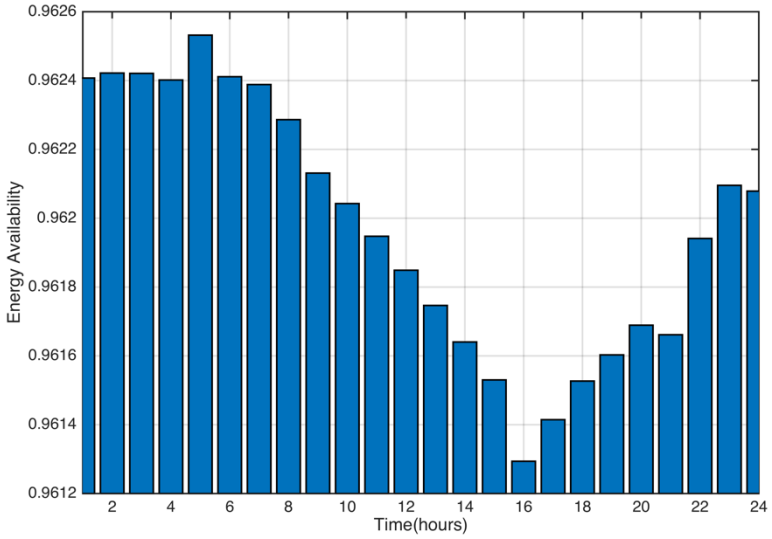

Figure 4-8 Energy availability for radial system

As we can see we can have the highest energy availability at 5:00 and the lowest energy availability at 16:00.

4.4 Case 2: Regional HVDC Transmission System

In this case, based on the wind speed and ambient temperature from a given 24-hour period, the energy availability for a regional system is calculated. The regional VSC-HVDC transmission is given below, and the reliability indices for components have already been given in 4.2.

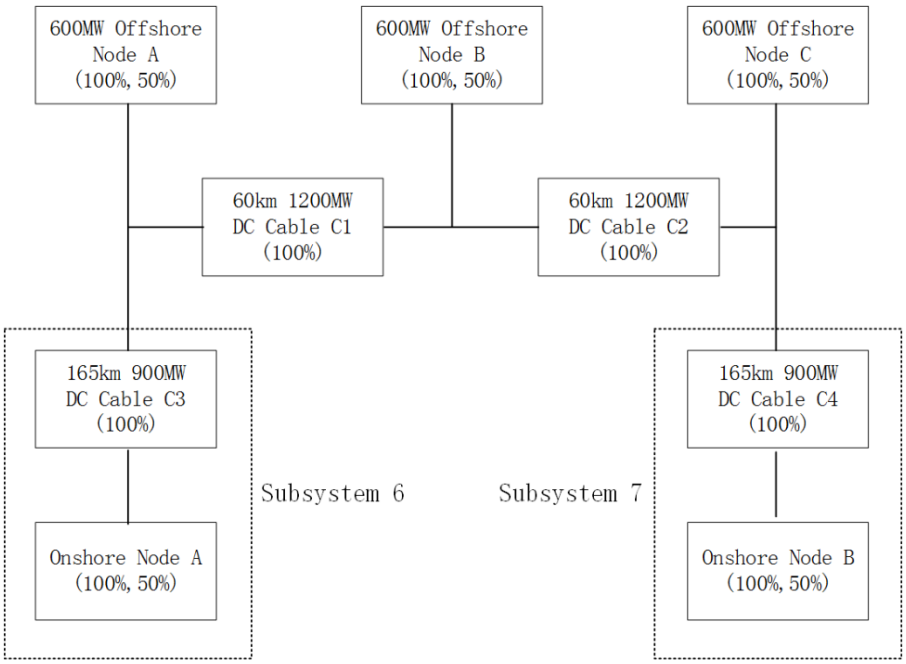

Figure 4-9 Regional VCS-HVDC transmission system

In this regional system, there are three offshore wind farms and two onshore stations. These three wind farms are connected by 60 km DC cables. Each of the offshore nodes (A, B, C) is a simplification of the subsystem 1 and onshore DC switchyard in case 1, and each of the onshore nodes (D, E) is a simplification of the subsystem 3 and onshore DC switchyard in case 1.

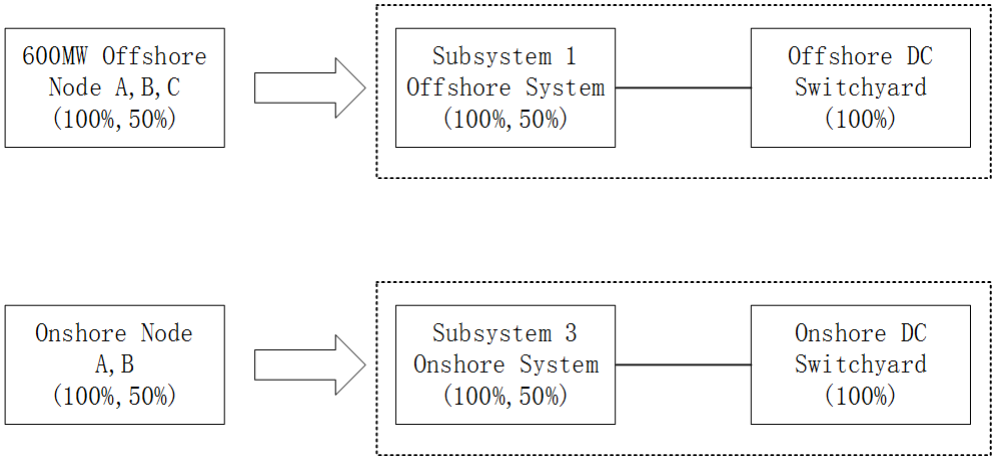

Figure 4-10 Simplification for offshore and onshore node

It can be further simplified as:

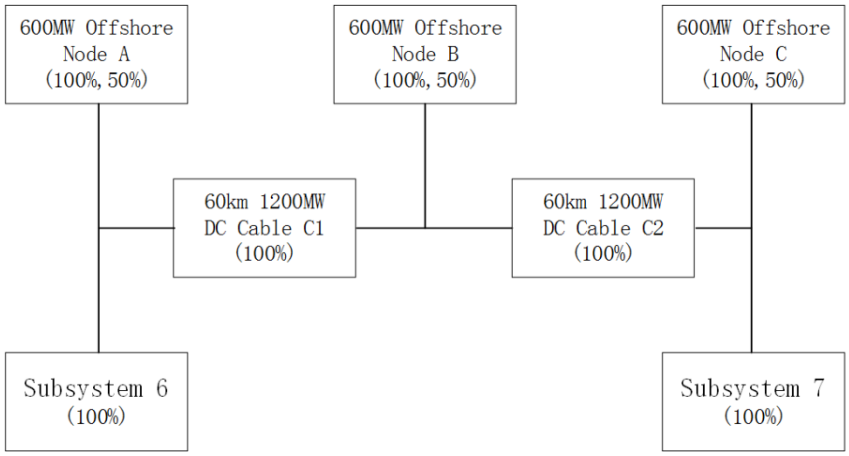

Figure 4-11 Simplification regional VCS-HVDC transmission system

The availability can be calculated with the same method as in case 1. A logic code is written to calculate the availability for this regional system.

In this case, we assume the installed capacity of each offshore wind farm is 600 MW, the transmission capacity of the DC cable between offshore nodes is 1200 MW, and the transmission ca-

pacity of the DC cable between offshore nodes to onshore nodes is 900 MW. The real-time availability for the subsystems and the energy availability for the whole system is calculated. The result is shown below:

Time	Offshore Node	Onshore Node	Energy Availability
1	0.97623022	0.98583695	0.96054097
2	0.97623426	0.9858477	0.96055509
3	0.97623387	0.98584719	0.96055424
4	0.97622773	0.98583372	0.96053548
5	0.97626638	0.98592812	0.96066264
6	0.97623015	0.98584099	0.96054474
7	0.97622399	0.98582395	0.96052257
8	0.97619232	0.98575138	0.96042293
9	0.97614604	0.98563907	0.96027139
10	0.97611925	0.9855754	0.96018496
11	0.97609057	0.98550696	0.96009217
12	0.97606088	0.98543587	0.95999589
13	0.97603015	0.98536204	0.95989601
14	0.97599833	0.98528536	0.95979238
15	0.97596538	0.98520572	0.95968484
16	0.97589511	0.98503439	0.95945414
17	0.97593063	0.98512238	0.95957208
18	0.97596369	0.98520401	0.95968159
19	0.97598919	0.98525618	0.95975582
20	0.97601501	0.98531854	0.95984004
21	0.97600562	0.98529964	0.959813
22	0.97609351	0.98549755	0.96008609
23	0.97613921	0.98560949	0.96023669
24	0.97613368	0.98559784	0.96022027

Table 4-8 Hourly availability for subsystems

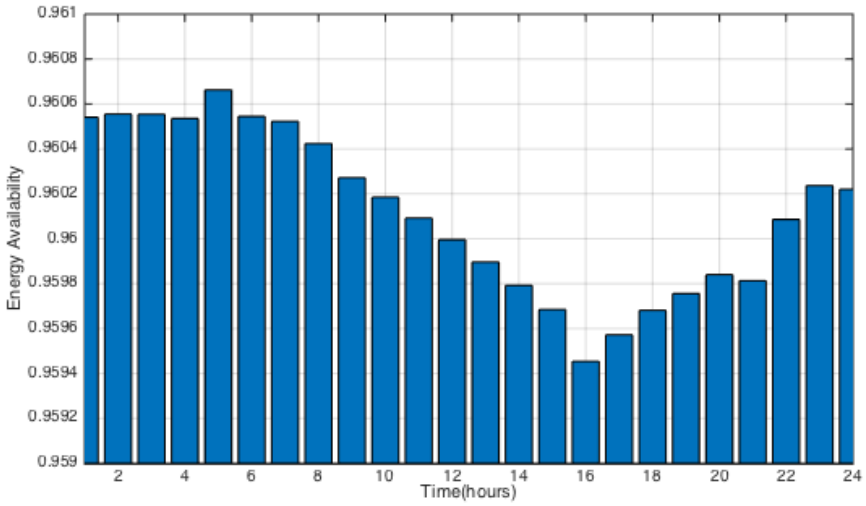

Figure 4-12 Energy availability for regional system

Again we can see the highest energy availability is at 5:00 and the lowest energy availability at 16:00. Take the availability at 16:00 as an example; for this regional transmission system, the energy availability for offshore nodes is 97.59%, the energy availability for onshore nodes is 98.50%. The total energy availability is 95.95%.

Although the regional scheme can have a more flexible transmission pass, when compared with case one at 16:00, the energy availability for the radial system is 96.13% and the energy availability for the regional system is 95.95%. The energy availability of the regional system in the 24-hour period is all lower then then the radial system. This is because of the capacity of the DC cable between the offshore nodes and onshore nodes. The reason will be further studied in chapter 5. The comparison of case 1 and case 2 is showed below.

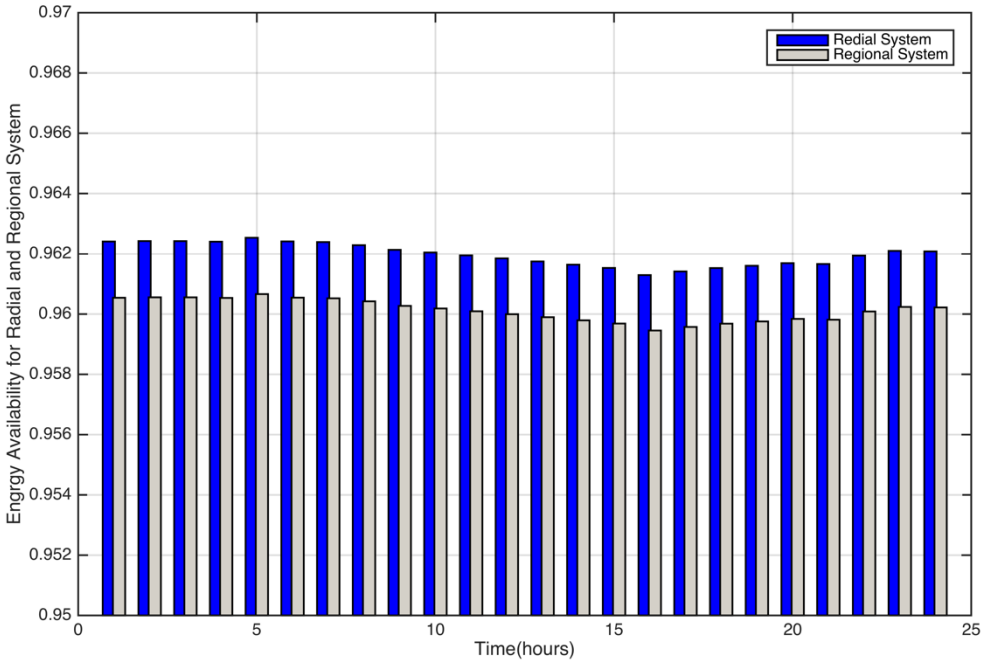

Figure 4-13 Energy availability comparison of case 1 and case 2

4.5Conclusions and Future Work

In this chapter, two cases were studied. In case 1, the real-time reliability for a radial system was calculated based on the converter model and the transformer model. In case 2, the real-time reliability for a regional system was calculated and the influence of DC cable capacity on system reliability is studied. In both of the cases, the reliability indexes for each component was discussed and the systems were simplified. The results show that, combining with the real-time failure rate model of the converter and the transformer, it can better reflect the reliability of the offshore wind power transmission system under the influence of wind speed and ambient temperature. When operating in the normal condition ambient temperature is the main factor to influence the system

reliability. A more flexible transmission path can increase the system reliability. And the capacity of DC cable should be adjusted.

Future work can be focused on the following aspects: analyze the contribution of each component to the system reliability; combining wind speed and temperature forecast technology to study the outage probability prediction of the transformer; combining with the economic analyze and choose the optimal scheme.

Chapter 5 Sensitivity Analysis

Based on the case study above, to evaluate the influence of the factors, a set of sensitivity analysis is done considering the following aspect:

1). Yearly real-time reliability calculation and seasonal characteristics;

2). The effect of wind turbine parameter setting;

3). The effect of DC cable capacity.

For these further calculation we choose the regional system in case 2 to do the system level reliability calculation

5.1 Yearly calculation and seasonal characteristics

To do this calculation, the hourly wind speed and ambient temperature data in whole year 2010 in Milwaukee is used.

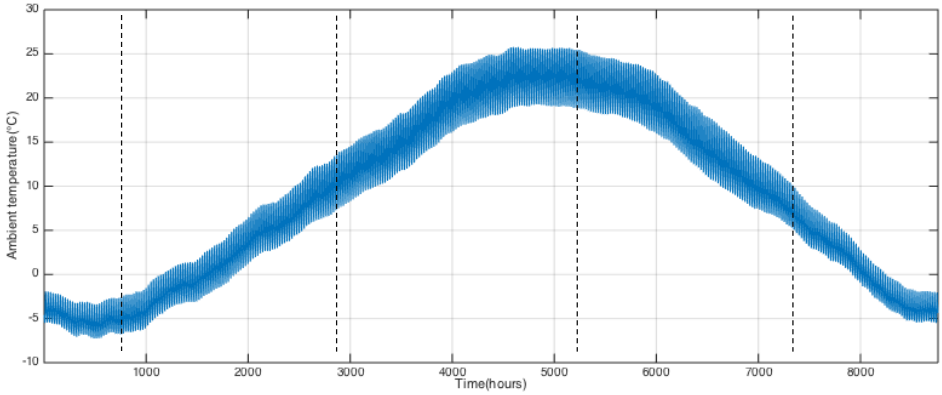

Figure 5-1 Ambient temperature in Milwaukee, 2010

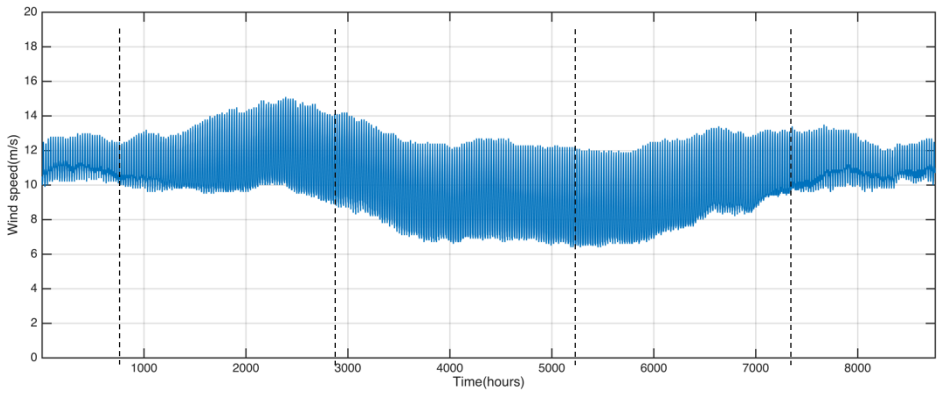

Figure 5-2 Wind speed in Milwaukee, 2010

As we can see above the wind speed and the ambient temperature have a specific seasonal character. For the ambient temperature, it has a relative high value in Summer and Autumn, and low value in Winter and Spring. For wind speed is just the opposite. And it is noteworthy that in the summer and autumn wind speed fluctuates more intense

Next, then the wind farm generation and the real-time availability for the converter and the transformer are calculated.

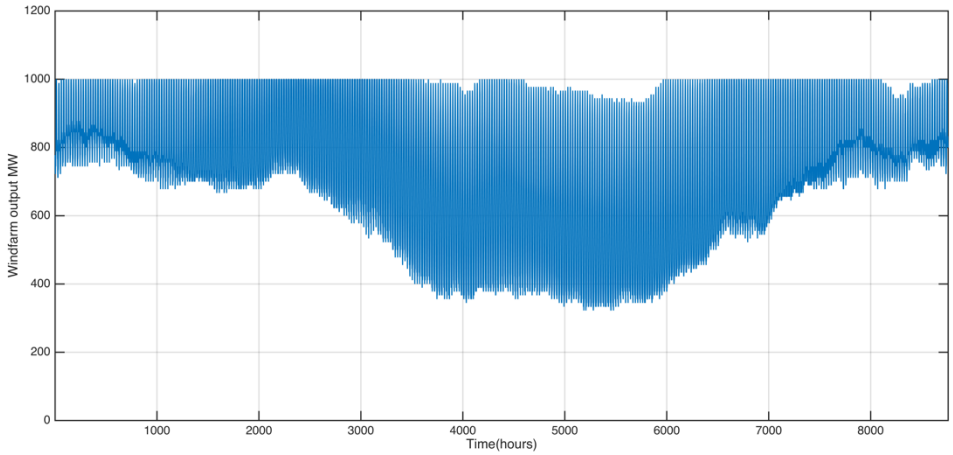

Figure 5-3 Hourly wind generation

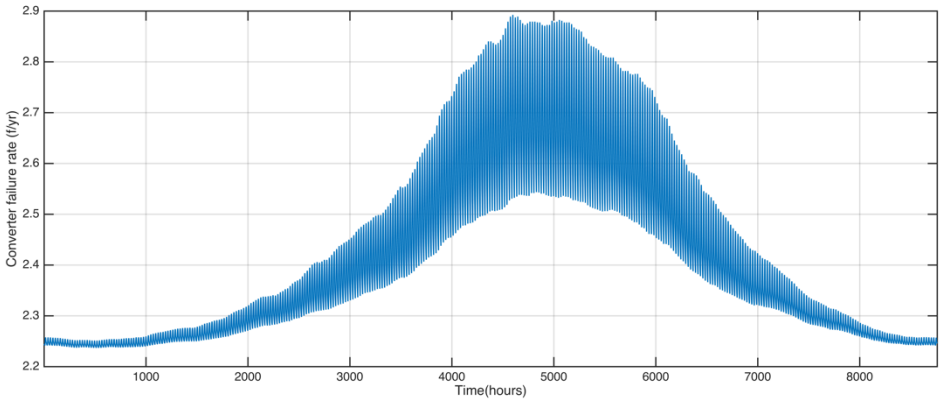

Figure 5-4 Hourly converter failure rate

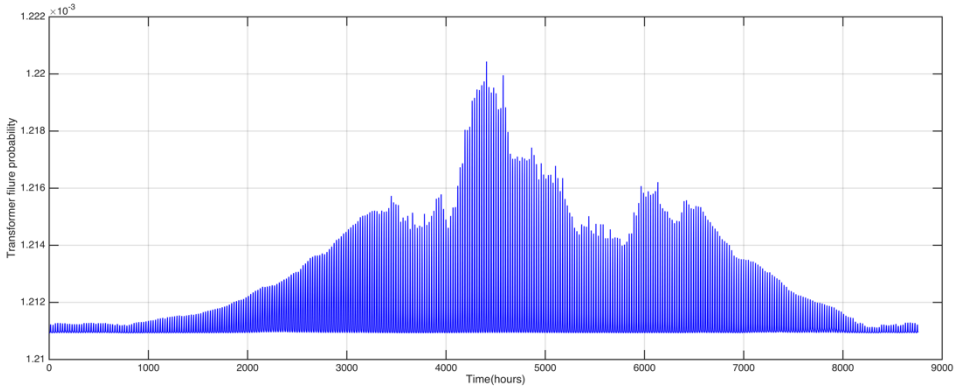

Figure 5-5 Hourly transformer outage probability

As we can see above, the lowest point for the wind generation is between 3000 hour to 6000 hour. This is because of the low wind speed during that period. Also the wind generation reflects the wind speed fluctuations in the summer and autumn. The trend of the hourly converter failure rate curve is consistent with the ambient temperature and it also reflects the fluctuation of the wind speed in summer and autumn. The trend of the hourly transformer failure probability curve is also consistent with the ambient temperature, the gaps in 3800 hour and 5500 hour correspond to the gaps of wind generation at that time.

Then the yearly real-time reliability for the regional system is calculated:

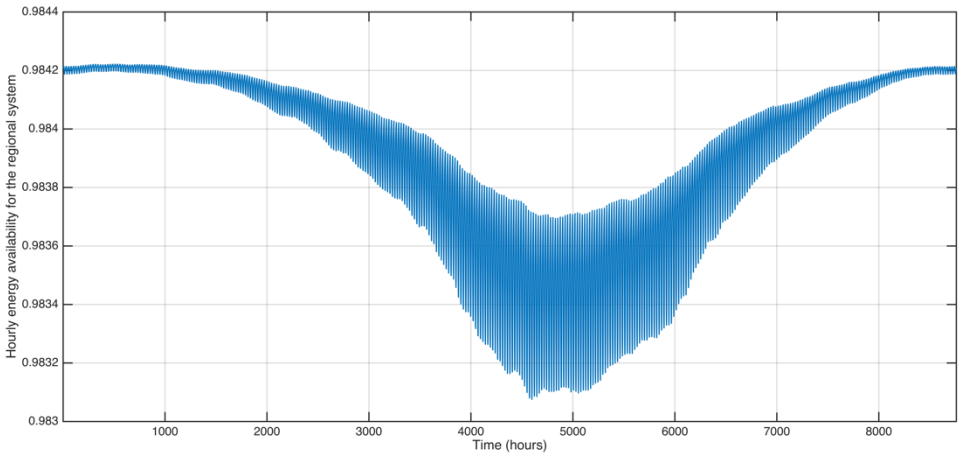

Figure 5-6 Hourly energy availability for regional system

As we can see above, the lowest energy availability is between 4000 hour to 6000 hour. It is in June and July when the temperature is highest in the year. Also, during that period of time the energy availability has the biggest fluctuation due to wind speed fluctuation.

5.2 The effect of wind turbine parameter setting

The parameters of the wind turbine, such as cut-in speed, cut-out speed and rated speed can affect not only the wind generation but also the reliability of the components. In this section the effect of cut-in speed is studied.

The cut-in speed will affect the wind generation and the wind generation will affect the reliability of converters and transformers. First, based on the 24-hour wind speed we used in the previous the average hourly wing generation was calculated as below:

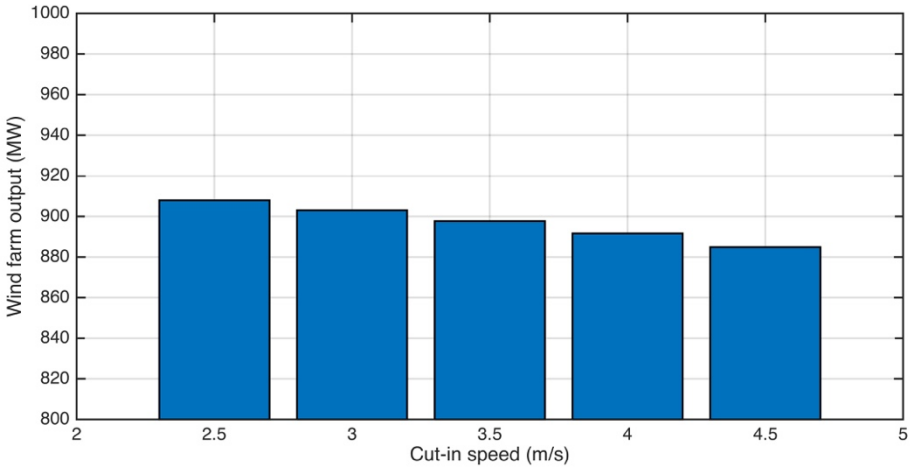

Figure 5-7 Average hourly wind generation

As we can see above, with the cut-in speed increase, the generation ability weakened. And the availability of the converter was also calculated:

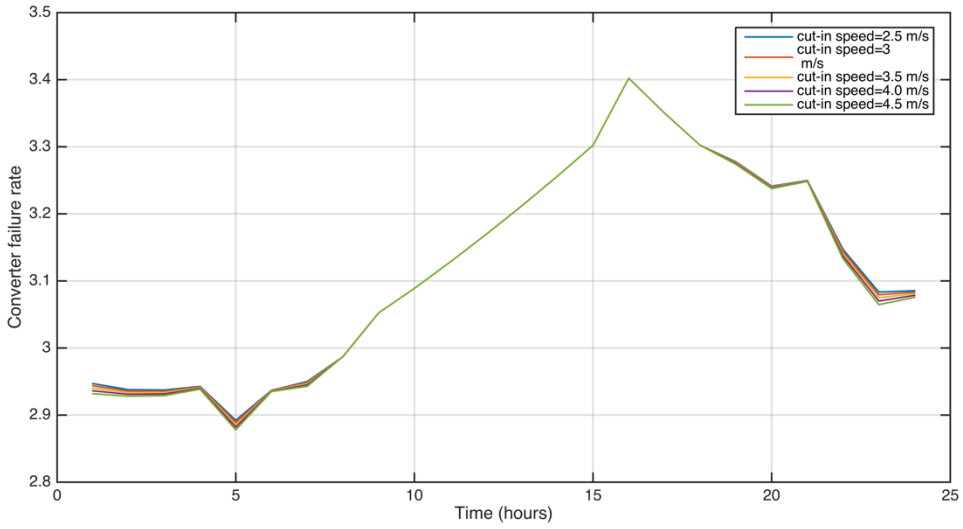

Figure 5-8 Converter failure rate

As we can see above the real-time failure for the converter is also influenced by the cut-in speed. When the wind speed is low, the effect is significant, when the wind speed reaches the rated speed there is no effect.

5.3The effect of DC cable capacity

In order to confirm the effect of DC cable capacity on system reliability, the capacity of the DC cable between the offshore nodes and onshore nodes was adjusted to 1200 MW and 1800 MW. As we can see, with the increase of the cable capacity, the energy availability also increased. The average energy availability for a regional system with two 900MW DC cables is 0.96012, for a regional system with two 1200MW DC cables is 0.96995, for a regional system with two 1800MW DC cables is 0.98463. This is because DC cables are the most important components in HVDC transmission system. The reliability of HVDC transmission system is largely depend on the reliability of DC cables. If we adjust the DC cable capacity to 1800 MW, one DC cable fault will not affect the energy availability.

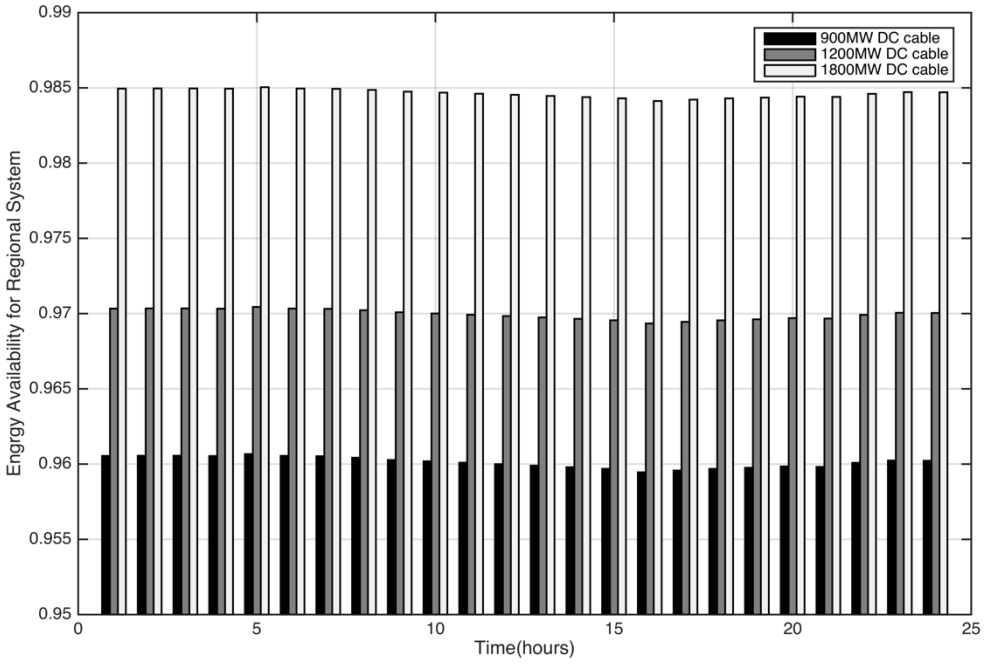

Figure 5-9 Energy availability for different DC cable capacities

Time	Regional		
	subsystem6 &7=900MW	subsystem6& 7=1200MW	subsystem6& 7=1800MW
1	0.96054	0.97033	0.98495
2	0.96056	0.97035	0.98496
3	0.96055	0.97034	0.98496
4	0.96054	0.97033	0.98495
5	0.96066	0.97044	0.98504
6	0.96054	0.97034	0.98495
7	0.96052	0.97032	0.98494
8	0.96042	0.97023	0.98486
9	0.96027	0.97009	0.98475
10	0.96018	0.97001	0.98468
11	0.96009	0.96993	0.98461
12	0.96000	0.96984	0.98454
13	0.95990	0.96975	0.98446
14	0.95979	0.96965	0.98439
15	0.95968	0.96956	0.98430
16	0.95945	0.96935	0.98413
17	0.95957	0.96945	0.98422
18	0.95968	0.96955	0.98430
19	0.95976	0.96962	0.98436
20	0.95984	0.96970	0.98442
21	0.95981	0.96967	0.98440
22	0.96009	0.96992	0.98460
23	0.96024	0.97005	0.98472
24	0.96022	0.97004	0.98471
AVE	0.96012	0.96995	0.98463

Table 5-1 Hourly energy availability for different DC cable capacities

5.4 Conclusions and Future Work

In this chapter, a set of sensitivity analysis is done considering the effect of wind turbine parameter setting and DC cable capacity. And the yearly reliability is calculated based on the yearly wind speed and ambient temperature data. The results show that, the seasonal characteristic is significant, and it is largely affected by the temperature. the wind speed also has its influences. The lowest system energy availability is in the hottest time of the year. A more flexible transmission path can increase the system reliability, if the capacity of DC cable is sufficient. To improve the system reliability, we can adjust the wind turbine parameters. Increase the capacity of the DC cable will also increase the system reliability.

Future work can be focused on the following aspects: analyze the optimal scheme considering the investment; calculating more reliability indexes considering the load. Considering the connection to the area distribution network.

Chapter 6 Conclusion

In this thesis, the operating reliability for the VSC-HVDC transmission system is studied. The reliability indexes for a radial and a regional offshore wind farm transmission systems are calculated.

Firstly, the converter real-time failure model and the transformer real-time failure model are built and tested. The results show that, with the real-time wind speed change, VSC failure rate and transformer failure probability will produce the corresponding change. The effect of ambient temperature on the failure rate of the converter is very significant in the stable operating environment. And the outage is more likely to happen during the daytime because of the high temperature. Even if the transformer is operating in the normal condition, the aging process will increase its outage probability slowly.

Then, systems are simplified by using the minimum cut set method. The reliability indexes for all components in the systems are set considering the difference between offshore and onshore environment. And the system energy availability is calculated for both system. The results show that, the availability for the system vary evidently with different operating and environment conditions. And the ambient temperature and the wind speed are the main factors.

Lastly, the sensitivity analyses study the influence of season, DC cable capacity, and wind turbine parameters. The results show that, the seasonal characteristic is significant, and it is largely affected by the temperature. the wind speed also has its influences. The lowest system energy availability is in the hottest time in the year. To improve the system reliability, we can adjust the wind turbine parameters. Increase the capacity of the DC cable will also increase the system reliability.

Future work can be focused on the following aspects:

- Considering more weather condition in components' failure model, and studying the impact of extreme weather on components' real-time failure and on system reliability;
- Building real-time failure rate model for other components in VSC-HVDC transmission system, such as switchyard, control system, transmission line and others.
- Integrating wind speed and temperature forecast technology; using the predication ambient temperature and wind speed to study the failure rate prediction of the system;
- Calculating the unavailability of each subsystem and analyzing the contribution of each component to the system reliability;
- Performing economic analysis; considering the investment and the maintenance to choose the optimal scheme.
- Calculating the system reliability for more systems with different topologies; and considering the connection to the area distribution network and calculating more reliability indexes with the load.

References

[1] International Energy Agency, “World Energy Outlook 2014 Executive Summary,” 2014.

[2] P. Bresesti, W. L. Kling, R. L. Hendriks, and R. Vailati, “HVDC connection of offshore wind farms to the transmission system,” *IEEE Trans. Energy Convers.*, vol. 22, no. 1, pp. 37–43, 2007.

[3] M. P. Bahrman and B. K. Johnson, “The ABCs of HVDC transmission technologies,” *IEEE Power Energy Mag.*, vol. 5, no. 2, pp. 32–44, 2007.

[4] K. R. Padiyar and N. Prabhu, “Modelling, control design and analysis of VSC based HVDC transmission systems,” *2004 Int. Conf. Power Syst. Technol. - POWERCON, Vols 1 2*, no. November, pp. 774–779, 2004.

[5] N. Flourentzou, V. G. Agelidis, and G. D. Demetriades, “VSC-Based HVDC Power Transmission Systems: An Overview,” *IEEE Trans. Power Electron.*, vol. 24, no. 3, pp. 592–602, 2009.

[6] G. Asplund, K. Eriksson, H. Jiang, J. Lindberg, R. Pålsson, and K. Svensson, “Dc Transmission Based on Voltage Source Converters,” *Proc. CIGRE SC14 Colloq. South Africa 1997*, 1997.

[7] S. G. Johansson, L. Carlsson, and G. Russberg, “Explore the power of HVDC light - a web based system interaction tutorial,” *IEEE PES Power Syst. Conf. Expo.*, pp. 839–842, 2004.

[8] A. Beddard and M. Barnes, “VSC-HVDC availability analysis,” *Univ. Manchester*, no. November, 2011.

[9] J. K. B. Dellby, G. Bergman, J. Karlstrand, “High-voltage cable technology,” *ABB Rev*, vol. 4, pp. 35–44, 2000.

[10] a. M. S. Atmadji and J. G. J. Sloot, “Hybrid switching: a review of current literature,” *Proc. EMPD ’98. 1998 Int. Conf. Energy Manag. Power Deliv. (Cat. No.98EX137)*, vol. 2, pp. 683–688, 1998.

[11] W. Energy, “Investigation on Reliability-driven Network Expansions of Offshore Transmission Systems,” 2016.

[12] B. Yang, “Reliability of parallel connected power transformers with failure correlation and its preventive maintenance,” *2014 17th Int. Conf. Electr. Mach. Syst. ICEMS 2014*, pp. 1044–1047, 2015.

[13] J. He, Y. Sun, P. Wang, and L. Cheng, “A hybrid conditions-dependent outage model of a transformer in reliability evaluation,” *IEEE Trans. Power Deliv.*, vol. 24, no. 4, pp. 2025–2033, 2009.

[14] R.Billinton and G.Singh, “Application of adverse and extreme adverse weather: Modeling in transmission and distribution system reliability evaluation,” *Proc. Inst. Elect. Eng., Gen., Transm. Distrib*, vol. 153, pp. 115–120, 2006.

[15] P. Wang and R. Billinton, “Reliability cost/worth assessment of distribution systems incorporating time-varying weather conditions and restoration resources,” *IEEE Trans. Power Deliv.*, vol. 17, no. 1, pp. 260–265, 2002.

[16] P. Wang and R. Billinton, “Time sequential distribution system reliability worth analysis considering time varying load and cost models,” *IEEE Trans. Power Deliv.*, vol. 14, no. 3, pp. 1046–1051, 1999.

[17] G. W. Swift *et al.*, “Adaptive transformer thermal overload protection,” *IEEE Trans. Power Deliv.*, vol. 16, no. 4, pp. 516–521, 2001.

[18] W. Fu, J. D. McCalley, and V. Vittal, “Risk assessment for transformer loading,” *IEEE Trans. Power Syst.*, vol. 16, no. 3, pp. 346–353, 2001.

[19] K. T. Muthanna, A. Sarkar, K. Das, and K. Waldner, “Transformer insulation life assessment,” *IEEE Trans. Power Deliv.*, vol. 21, no. 1, pp. 150–156, 2006.

[20] Y. Sun, P. Wang, L. Cheng, and H. Liu, “Operational reliability assessment of power systems considering condition-dependent failure rate,” *Gener. Transm. Distrib. IET*, vol. 4, no. 1, pp. 60–72, 2010.

[21] Y. S. Y. Sun, L. C. L. Cheng, H. L. H. Liu, and S. H. S. He, “Power system operational reliability evaluation based on real-time operating state,” *2005 Int. Power Eng. Conf.*, 2005.

[22] K. Xie, B. Hu, and C. Singh, “Reliability Evaluation of Double 12-Pulse Ultra HVDC Transmission Systems,” *IEEE Trans. Power Deliv.*, vol. 31, no. 1, pp. 210–218, 2016.

[23] R. Billinton and R. N. Allan, *Reliability Evaluation of Power Systems*. 1996.

[24] S. Kuruganty, “Effect of HVDC component enhancement on the overall system reliability performance,” *IEEE Trans. Power Deliv.*, vol. 9, no. 1, pp. 343–351, 1994.

[25] R. Billinton, M. Fotuhi-Firuzabad, and S. O. Faried, “Reliability evaluation of hybrid multiterminal HVDC subtransmission systems,” *IEE Proc. - Gener. Transm. Distrib.*, vol. 149, no. 5, p. 571, 2002.

[26] C. Maciver, K. R. W. Bell, and D. P. Nedic, “A reliability evaluation of offshore HVDC grid configuration options,” *IEEE Trans. Power Deliv.*, vol. 31, no. 2, pp. 810–819, 2016.

[27] S. Zadkhast, M. Fotuhi-Firuzabad, F. Aminifar, R. Billinton, S. O. Faried, and A. A. Edris, “Reliability evaluation of an HVDC transmission system tapped by a VSC station,” *IEEE Trans. Power Deliv.*, vol. 25, no. 3, pp. 1962–1970, 2010.

[28] Y. Li, F. Liu, L. Luo, C. Rehtanz, and Y. Cao, “Enhancement of commutation reliability of an HVDC inverter by means of an inductive filtering method,” *IEEE Trans. Power Electron.*, vol. 28, no. 11, pp. 4917–4929, 2013.

[29] M. Arifujjaman, M. T. Iqbal, and J. E. Quaicoe, “Reliability analysis of grid connected small wind turbine power electronics,” *Appl. Energy*, vol. 86, no. 9, pp. 1617–1623, 2009.

[30] L. Wang, “No Reliability Evaluation of an HVDC Transmission System Considering the Influence of Power Electronics,” 2016.

[31] D. a Murdock, J. E. R. Torres, J. J. Connors, and R. D. Lorenz, “Active thermal control of power electronic modules,” *Ind. Appl. IEEE Trans.*, vol. 42, no. 2, pp. 552–558, 2006.

[32] X. Xu, J. Mitra, T. Wang, and L. Mu, “Evaluation of operational reliability of a microgrid using a short-term outage model,” *IEEE Trans. Power Syst.*, vol. 29, no. 5, pp. 2238–2247, 2014.

[33] K. Xie, Z. Jiang, and W. Li, “Effect of Wind Speed on Wind Turbine Power,” vol. 27, no. 1, pp. 96–104, 2012.

[34] H. Zhang and L. M. Tolbert, “Efficiency impact of silicon carbide power electronics for modern wind turbine full scale frequency converter,” *IEEE Trans. Ind. Electron.*, vol. 58, no. 1, pp. 21–28, 2011.

[35] T. Committee, *IEEE C57.91-1995 Guide for Loading Mineral-Oil- Immersed Transformers*, vol. 1995. 1995.

[36] T. Weekes, T. Molinski, and G. Swift, “Transient transformer overload ratings and protection,” *IEEE Electr. Insul. Mag.*, vol. 20, no. 2, pp. 32–35, 2004.

[37] P. K. Sen and S. P. S. Pansuwan, “Overloading and loss-of-life assessment guidelines of oil-cooled\ntransformers,” *2001 Rural Electr. Power Conf. Pap. Present. 45th Annu. Conf. (Cat. No.01CH37214)*, pp. 1–8, 2001.

[38] W. J. McNutt, “Insulation Thermal Life Considerations for Transformer Loading Guides,” *IEEE Trans. Power Deliv.*, vol. 7, no. 1, pp. 392–401, 1992.

[39] D. J. Groebel, A. Mettas, and F.-B. Sun, “Determination and interpretation of activation energy using accelerated-test data,” in *Annual Reliability and Maintainability Symposium. 2001 Proceedings.*, 2001, pp. 58–63.

[40] E. Engineers, T. P. Avenue, S. Licensing, and S. Licensing, *Draft IEEE Guide for Protecting Power Transformers*, vol. 2008, no. May. 2006.